Polymer solar cells

Jacob Lund Rasmus Røge René Petersen Tom Larsen

1st June 2006

AALBORG UNIVERSITY
FACULTY OF PHYSICS AND NANOTECHNOLOGY

Skjernvej 4C ▪ DK-9220 Aalborg Øst

Title: Polymer Solar Cells
Project Period: 2^{nd} of February 2006 - 31^{st} of May 2006
Project Group: N440B

Project group:
Rasmus E. Røge
Tom Larsen
René Petersen
Jacob Lund

Contact:
aauprojects@repetit.dk

Supervisor:
Thomas G. Pedersen
Peter Kjær Kristensen

Synopsis

This project is based on the initial problem - "How can polymer solar cells be produced and characterized". Polymer solar cells are a much cheaper and easier produced alternative to traditional silicon solar cells. In this project the underlying physical principles of polymer solar cells was investigated. This includes a description of the conjugated polymers used in polymer solar cells. The effect of the field strength and the binding energy on charge separation was theoretically briefly investigated. Through a tight binding model and the Simple Hückel Method a computer program for calculating the band structure and absorbance spectrum of conjugated polymers was made. Polymer solar cells of the type ITO/PEDOT:PSS/MEH-PPV:PCBM/Al was produced and tested. The effect of PEDOT:PSS on the performance of the cells was tested. The cells was characterized by recording their IV curve and measuring V_{OC} and I_{SC}.

Circulation: 8
Number Of Pages: 99
Finished: 29^{th} of May 2006

Preface

This report is the product of the 4^{th} semester project period on the nanotechnology education on Aalborg University, Denmark. The report is addressed to people with an interest in alternative power sources, and with a basic knowledge in quantum mechanics. It is typeset in LaTeX2e.

The report is divided into chapters, sections and subsections. The first chapter "Introduction" gives a basis knowledge of solar cells and introduces the polymer solar cell. The chapter "Problem Analysis" explains the physical principles behind photovoltaic devices, and creates a baseline for the report. "Theoretical Foundation" is the first step into calculations and explanations of the behavior of the polymer solar cell."Software - EBCalc" describes the functionality and development of the program EBCalc. "Materials and Methods" describes the experimental part of the project. "Results" is the presentation of the results obtained. "Discussion" and "Conclusion" discusses and concludes on the results obtained. "Appendix"tread some specific subject in greater details. We would like to thank:

- Kim Houtved Jensen and Barbara Samuelsen Hansen, laboratory assistant at the institute of Physics and Nanotechnology at Aalborg University. For help and assistance during the project period.
- Frederik Christian Krebs, Senior Scientist at Risø National Laboratory. For an introduction to polymer solar cells, and assistance during the project period.
- Group 4.42. for assisting in equipment setup and for good cooperation.

A Note on Notation

Matrices and vectors are written using bold font. Matrices are displayed in uppercase characters and vectors are lowercase, unless otherwise specified ($\mathbf{A}$, $\mathbf{v}$). Operators are written in normal uppercase font with a hat above ($\hat{H}$)

Enclosed CD

Located on the enclosed CD are the program executable and the program source code. The .pdf version of the report, the data obtained and the mathematica files used for calculations are also located on the CD.

Contents

Chapter 1

Introduction

The Sun is providing the Earth with an enormous amount of energy, approximately 200'000 times the capacity of the total energy production facilities. Only a very small amount of this energy is used. Hence the thought of developing a device that effectively and cheaply harvests the solar energy is very attractive.

There is a line of problems connected with using the solar energy. Firstly the averaged yearly local intensity is varying from less than $100Wm^{-2}$ to a little more than $300Wm^{-2}$. This means that sunlight must be collected over a very large area in order to produce an amount of electrical energy comparable with that consumed by a city, fabric or even a house.

Secondly the energy of the sunlight cannot be directly used in any way. Therefore, turning the radiative solar energy into a more useable energy type is the primary objective. There exists two different approaches to this problem but with either approach a rather large amount of the radiative energy is lost in the conversion.

- Conversion into thermal energy.
- Conversion into electrical energy.

The solar light is converted into thermal energy when interacting with matter. This can be used for heating water and house warming etc. The applications are naturally limited as a very large part of our energy consumption is electrical energy. [Britannica, 2006]

The silicon solar cell (SSC) has been and is the most used way to convert solar energy into electrical energy. A short summary of the history and basic physical principles of the silicon solar cells is presented in the following sections.

1.1 Silicon Solar Cells

The silicon solar cell is the traditional solar cell and has found applications in various areas such as calculators, garden lamps, and roofmounted large area cells etc. The SSC has so far been the best candidate for conversion of sunlight and therefore the developement and research of solar cells has been dominated by this.

SSCs trace their history back to the 1950s where the first SSC was reported by Chapin, Fuller and Pearson. It had a power conversion efficiency of 6%. The price per watt was very high, being as much as $ 200 per watt. This meant that SSCs were not seriously considered as an everyday power source for many decades, only in very remote places and if the costs was made unimportant by the benefits of SSCs, e.g. satellites.[Nelson, 2003]

SSCs has benefited from the fast development in the integrated circuit industry, and this means that it is now possible to produce SSCs with efficiencies as high as 25%, and at a much lower cost than previously [Shah et al., 1999]. The prices for solar cell power today lies between $ 10 and 12 W^{-1}, based on todays prices on the internet.[Elektronikbutikken, 2006]

1.2 Introduction to the Physics of Solar Cells

Silicon solar cells are based on the physical principles described by Planck's law. This law states that the energy of a single photon is equal to $h\nu$, where h is Planck's constant and ν is the frequency of the light. The energy is thus proportional to the frequency and inversely proportional to the wavelength.

When light, with a frequency corresponding to an energy larger than the band gap, hits a semiconductor like silicon some of the electrons are excited into higher energy levels. Only if the energy of the photons are larger than the band gap, the electron can be excited. If the energy is much larger than the band gap the electron can be ejected from the material. This is known as the photoelectric effect. In these excited states the electrons are more free to move, and can thus lead a current if a potential difference is imposed across the cell. This potential difference arises from a built in asymmetry in the cell.

SSCs are built from several different layers, two of them being n-type silicon (negative - excess of electrons) and p-type silicon (positive - excess of holes). Naturally found silicon has 14 electrons, 4 of them being valence electrons. In the solid state silicon forms covalent bonds with four neighboring silicon atoms, and this forms the crystal lattice. To create n-type and p-type silicon, impurities are introduced into the crystal lattice. This controlled and on purpose contamination of silicon is known as doping. N-type silicon can be created by doping with phosphorus.

Phosphorus is incorporated into the crystal lattice where it occupies a lattice point which would otherwise be occupied by a silicon atom. Because phosphorus contains five valence electrons, and only four of them are used for bonding, there is one excess electron per unit cell. Similarly, to create p-type silicon, atoms with three valence electrons, for example boron, are incorporated into the lattice producing an excess amount of holes. A more detailed description of doping can be found in Appendix A.

When p-type and n-type silicon are brought together a p/n junction is formed at the interface. Because of the excess of electrons on one side, and the excess of holes on the other side electrons and holes recombine at the junction, creating an insulating junction which is termed the depletion zone. When electrons flow from the n-type side towards the junction, excess positive charge is left behind. Similarly, excess negative charge is left behind when holes flow to the junction. This excess charge is not free to move because it is part of the chemical bonds between atoms. As a result an electric field directed from the n-type side to the p-type side is established. This is illustrated in Figure 1.1. A more extended description of this pn junction can be found in Appendix B

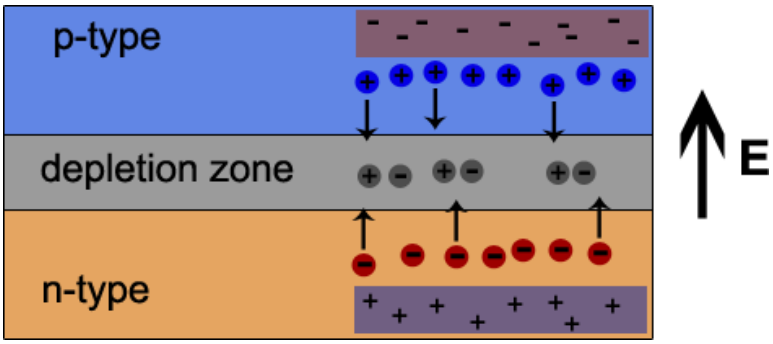

Figure 1.1: Illustration of the depletion layer. When the p-type and n-type layer are brought together, electrons from the n-type side recombine with holes from the p-type side at the depletion layer. The depletion layer is therefore an insulating layer because there are no free charge carriers

A basic SSC unit produces a photovoltage of between 0.5 and 1.0 volt and a photocurrent of some tens of milliamps per cm^2 when illuminated by the sun. This voltage is too small for most applications and therefore multiple cells are connected in series into *modules*. [Nelson, 2003]

Although the manufacturing costs of SSCs have dropped dramatically since the first cells was produced in the 1950's, the costs are still too high for large scale energy production. Furthermore, the production is not an easy task, the SSCs are not very flexible and silicon is in great demand due to the ever growing computer industry. This is not subject to change, therefore different paths must be examined.

1.3 Polymer Solar Cells

Polymer solar cells (PSC) is one of the possible replacements. These solar cells add some very interesting properties to the solar cell as well as reducing the price considerably. [Krebs et al., 2004] have demonstrated that the production of large area PSC ($1m^2$) can be done at a cost 100 times lower than that of monocrystalline silicon solar cells in terms of material cost.

Another area where the PSC has advantages over silicon cells is in flexibility. Whereas silicon crystal is rigid a polymer layer is very flexible yielding the possibility of a very flexible thin film solar cell. This is a property that can enable a variety of new applications, solar cell coated clothes has been demonstrated on Risø [Krebs, 2006].

However there are still challenges to overcome. Firstly the service life of a PSC is very short, only a few hours for a simple metal/polymer/metal solar cell. Secondly the efficiency of the PSC is not high compared to the SSCs. PSCs has power conversion efficiencies around 3% using different optimization methods.[Spanggaard and Krebs, 2004]

This leads us to our initiating problem:

- How can polymer cells be produced and characterized.

Chapter 2

Problem Analysis

Before a polymer solar cell can be produced and before its ability to convert solar energy into electricity can be analyzed, is it crucial to get an insight into how a polymer solar cell is constructed and how it functions. The purpose of this chapter is to describe polymer solar cells and introduce the physical principles behind it.

This chapter starts with a brief introduction to the type of solar cell which is treated in this report. The structure of the solar cell and the solar spectrum are described. The problem analysis is concluded with project limitations and project statement.

2.1 Polymer Solar Cells

During the last 30 years the polymer solar cell has developed from an inefficient light-harvesting device with almost no lifetime to a device that may be introduced to the commercial marked within a short span of years.

Today scientists are working with a lot of different types of polymer solar cells and since it will be too comprehensive to deal with all of them, only one type will be treated in this report. The type of solar cell which will be treated is a polymer/fullerene bulk heterojunction solar cell, and a schematic illustration of it can be seen in Figure 2.1.

This type of polymer solar cell consist of five layers: Glass, ITO, PEDOT:PSS, active layer, calcium and aluminum.

The glass serves as a supporting layer for the solar cell and the only demand glass has to fulfill is that it does not absorb light in the visible area, since the solar cell uses this light to generate power. Other and more flexible types of supporting layers, like transparent polymers, can also be used. The focus of this report will not lie on the supporting layer and therefore the use of other types of supporting layers will not be discussed any further.

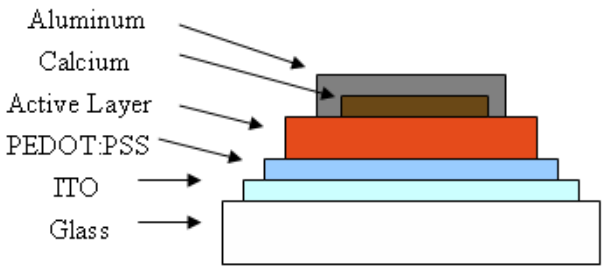

Figure 2.1: The structure of a polymer solar cell

ITO (indium tin oxide) and aluminum serves as the electrodes in the solar cell. Beyond that, the ITO and aluminium are also used to generate a built-in electric field caused by the difference in the metals' work functions. This electric field is used dissociate the excitons, which are generated when the active layer absorbs light, and afterwards to pull the charge carriers out from the active layer. Like glass the ITO layer is transparent in the visible area.

PEDOT:PSS (poly[3,4-(ethylenedioxy)-thiophene]:poly(styrene sulfonate)) and calcium are two materials which are introduced into the solar cell in order to increase the built-in electric field and thereby improve the performance of the solar cell.[Sigma-Aldrich, 2006]

The active layer in this polymer solar cell consists of a blend between the conjugated polymer MEH-PPV ((poly[2-methoxy-5-(2-ethylhexyloxy)-1,4-phenylenevinylene])) and the modified fullerene PCBM (1-(3-Methoxy-carbonylpropyl)-1-phenyl-[6.6]C61) [American Dye Source, 2006]. MEH-PPV is the absorbing part of the active layer and PCBM is introduced into the layer to make the dissociation of the excitons more effective.

This section was just an introduction to the polymer solar cell which will be analyzed more carefully throughout the rest of this report.

2.2 The Built-in Electrostatic Field

When an exciton has been generated in a polymer solar cell it has to be dissociated into an electron and a hole and these two charges carriers have to reach different electrodes before the device can deliver any current to an external circuit. To achieve this, the polymer solar cell must have some kind of built-in driving force which can accumulate the dissociations and generate a charge transport.

This built-in driving force can be created trough spatial variations in the electronic environment, which practically is done through junctions between of materials with different electronic properties.[Nelson, 2003]

In the simplest polymer solar cell, the polymer layer is sandwiched between two metals forming a heterojunction. The two metals establish an electric field inside the polymer caused by their asymmetrical work functions. This electric field can be used to dissociate the generated excitons since it pulls the electrons and holes in opposite direction.[Spanggaard and Krebs, 2004]

The work function of a metal is defined as the difference in potential energy of an electron in the vacuum level and in the Fermi level of a metal. The vacuum level is the energy of an electron a rest at a point infinitely far away from the metal. The Fermi level describes the energy of the least tightly held electron in the material.[Kittel, 2005]

The shape of the valence and the conduction band, when the polymer and the metallic electrodes are put into contact, depends on the conductance of the polymer and on whether the polymer solar cell is assembled or not, see Figure 2.2. Before the polymer solar cell is assembled the Fermi levels of the two electrodes are independent of each other. When the polymer solar cell is assembled a redistribution of the charge carriers starts. The charge carriers continue to diffuse until the Fermi levels have aligned in the two metals and a thermal equilibrium has been reached. The redistribution of charges lead to an establishment of an electric field, which affects the valence and conduction bands in the polymer. Dependent on the conductivity of the polymer two different profiles of the bands can be created.[Archer and Hill, 2001]

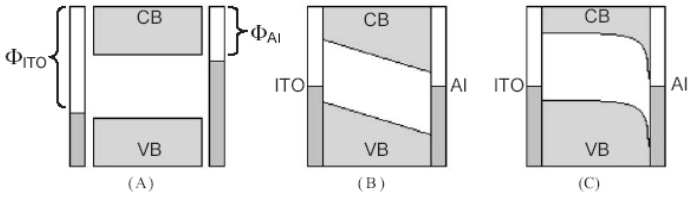

Figure 2.2: Shows the energy levels in a polymer solar cell. ITO is used as the high work function electrode and Al is used as the low work function electrode. (a) displays the energy levels before the polymer solar cell is assembled. (b and c) shows the energy levels after assembling. In (b) the polymer is an isolator and therefore the electric field changes linearly through the cell. The polymer used in (c) is a hole conducting polymer and therefor a Schottky junction will be formed between the polymer and the low work function electrode. [Spanggaard and Krebs, 2004]

If the polymer is an isolator, it will not have any free charges carriers. Therefore only charge carriers from the electrodes can diffuse. Electrons from the low work function electrode diffuse to the high work function electrode in order to align the Fermi levels and establish a thermal equilibrium. This leaves the low work function electrode positively charged and the high work function electrode negatively charged. This potential

difference between the two electrodes results in a generation of an electric field. This field changes linearly throughout the solar cell and thereby pulling the valence and conducting band in the polymer skew, see Figure 2.2.[Archer and Hill, 2001]

This band bending does not refer to a physical bending of the valence and conduction band. It is used to illustrate a local change in the energy of electrons in a semiconductor caused by an applied electric field. It is pictured in this way because the normal way to visualize the electron energy states and Fermi level in a material is to draw bands on an energy vs. distance plot.

When the polymer is a hole-conducting semiconductor, which is often the case since most polymers are better hole conductors than electron conductors, the shape of the valence and conduction band looks different. Due to the hole conducting properties of the polymer, holes are free to redistribute in the polymer and therefore they participate in the alignment of the Fermi levels. At the junction between the polymer and the low work function electrode, holes from the polymer will diffuse into the electrode in order to lower their energy. This diffusion of holes leaves a region of negatively charged acceptor atoms behind in the polymer and creates a positively charged region in the electrode. Through this establishing of an electric field, the valence and conduction band in the polymer close to the junction between the polymer and the low work junction electrode is bent, see Figure 2.2. If the polymer was an electron conductor, the band bending would have occurred at the junction between the polymer and the high work function electrode. This type of junction is normally referred to as a Schottky junction.[Archer and Hill, 2001]

The distance over which the valence and conduction band is bent is called the depletion width and it varies in the two cases. When the polymer is an isolator, the depletion width is as wide as the polymer layer. In a Schottky junction the depletion width is only a few nanometers.[Spanggaard and Krebs, 2004]

2.2.1 Improvements of the Built-in Field

In the previous section it was mentioned that the built-in electric field is created due to the difference in the work function of the two electrodes. Therefore it is important to be aware of what types of metals that are chosen as the electrodes.

In a simple polymer solar cell ITO (indium tin oxide) and aluminium are often used as the high and low work function electrode, respectively. In the literature the work function of ITO is listed to be between 4.4 and 5.14 eV. The reason for this varying value of the work function can be addressed to the production of the ITO layer, where changes in the production procedure results in different work functions.[Park et al., 1996] The work function of aluminum is listed to be 4.2 eV [CRC, 2006].

To improve the establishment of the built-in field other materials can be introduced into the polymer solar cell. PEDOT:PSS is often put in between ITO and the active layer, because of its high work function of 5.2 eV, which also is more homogeneous compared to the work function of an ITO layer. The PEDOT:PSS layer will also lower the risk for short circuiting, since the PEDOT:PSS layer is smoother than the ITO layer. Furthermore PEDOT:PSS is used as an electron barrier since PEDOT:PSS is a hole conductor, which also gives an improvement at the high work function electrode.[Mihailetchi et al., 2003]

At the low work function electrode calcium can be introduced in between the active layer and Al layer. The work function of calcium is 2.9 eV [CRC, 2006]. When calcium is used the aluminium layer also serves as a protective shell, since calcium reacts strongly with the constituents of the atmosphere.

If PEDOT:PSS and calcium is used at the high and low work function electrode, the maximum potential difference, which can be established when the Fermi levels align, is the difference in work function divided by an elementary charge. This gives a maximum voltage of 2.3 V, where the voltage between ITO and aluminium can differ a lot depending on the actual work function of the ITO layer, but a maximum voltage would be 1.33 V.

2.3 Heterojunction Between Donor and Acceptor Molecules

Previously it has been mentioned that the built-in electric field is used to dissociate the generated excitons into holes and electrons. Afterwards it pulls the charges to their respective electrodes. It has been shown that the dissociation is most effective at the two interfaces and that this dissociation is in fact an inefficient process. Therefore improvements have to be made in order to make polymer solar cells more efficient. [Archer and Hill, 2001]

In the early 1950's it was reported for the first time that the dissociation of excitons is efficient at the interface between certain semiconducting materials with different ionization energy and electron affinity. In order to optimize the exciton dissociation, in polymer solar cells, this was tested, with success. An illustration of the principle behind the separation can be seen in Figure 2.3. [Archer and Hill, 2001]

In this type of polymer solar cell a heterojunction between donor molecules and acceptor molecules is made. When a donor molecule is excited by the sunlight an electron is raised from the HOMO (highest occupied molecular orbital) to the LUMO (lowest unoccupied molecular orbital) and it leaves a hole behind. This excited electron has two opportunities; it can recombine with a hole under emission of a photon or it can separate

from the hole. When the LUMO of the acceptor molecule is lower than the LUMO of the donor molecule, the excited electron can relax into the LUMO of the acceptor molecule. If this happens the excited electrons will be separated from the hole and both charges can contribute to the total current produced by the polymer solar cell. The hole will travel in the donor molecule and the electron in the acceptor molecule to their respective electrodes.[Spanggaard and Krebs, 2004]

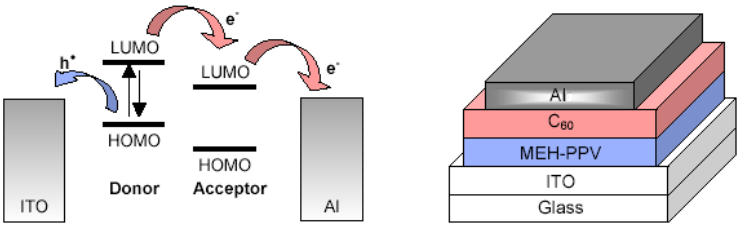

Figure 2.3: (left) Exciton dissociation at a donor-acceptor interface. (right)A polymer solar cell which makes use of a heterojunction between PCBM and MEH-PPV layers. Modified from [Spanggaard and Krebs, 2004]

When a heterojunction is made it is important to be aware that the diffusion length of an exciton in most polymers is short, actually in the range of 10 nm. This short diffusion length limits the thickness of the photon absorbing layer. A very thin absorbing layer however impose another problem, because most organic semiconductors absorb light poorly when the layer is only 10 nm thick. This means that few excitons are generated. In fact the layer should be approximately 100 nm thick in order to absorb most of the light, but then the majority of the excitons will recombine before they reach the interface. This problem can be solved by a concept called bulk heterojunction where the donor and acceptor molecule is blended.[Spanggaard and Krebs, 2004]

In this blend there will be heterojunctions distributed throughout the layer, which decreases the length an exciton has to travel before it enters a junction.

The polymer solar cell treated in this report utilizes a bulk heterojunction between MEH-PPV and PCBM. MEH-PPV is the donor molecule and PBCM is the acceptor molecule.

MEH-PPV and PBCM will be described in more details in the next section together with ITO and PEDOT:PSS.

2.4 The Materials of an Organic Solar Cell

In this section MEH-PPV, PEDOT:PSS, PCBM, and ITO will be described. A figure representing the molecule or the monomer of the polymer will be added for each material and an absorbance-curve for each of the materials will be described.

2.4.1 MEH-PPV

MEH-PPV(Poly[2-methoxy-5-(2-ethyl-hexyloxy)-1,4-phenylenevinylene])seen in Figure 2.4 is the active material of the solar cell. It is a modification of PPV, modified by the MEH-group, which makes it more soluble in some liquids, among those are THF(tetrahydrofuran).

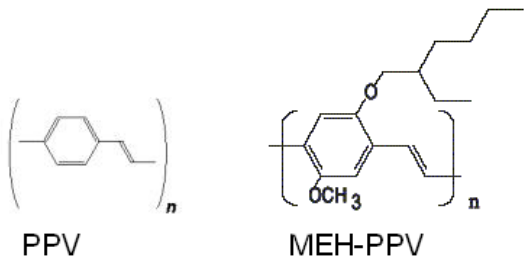

Figure 2.4: The two figures is the monomer of MEH-PPV(right) and the monomer of PPV(left)

2.4.2 PEDOT:PSS

PEDOT:PSS(Poly(2,3-dihydrothieno-1,4-dioxin)/poly(styrenesulfonate)) seen in Figure 2.5, is a polymer added to the solar cell to increase the electric field strength and improve the junction at the high workfunction electrode. PSS makes PEDOT soluble in water and dopes it.

2.4.3 PCBM

PCBM(1-(3-Methoxycarbonylpropyl)-1-phenyl-[6.6]C61) seen in Figure 2.6 is a modification of C_{60} The modification makes it more soluble in organic solvents. PCBM has the function as an electron acceptor in the solar cell.

2.4.4 ITO

ITO(Indium Tin Oxide)is a transparent conductive material. It is a mixture of indium oxide(In_2O_3) and tin oxide (SnO_2). ITO is used as one of the electrodes in the solar cell.

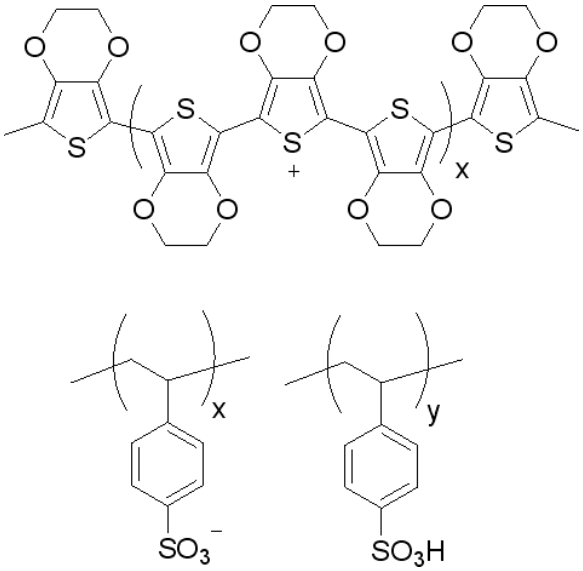

Figure 2.5: The figure shows PEDOT:PSS, where the upper part of the figure is PEDOT and the lower part named X is PSS where an electron from PEDOT has been moved to PSS. The lower part named Y is the normal structure for PSS[Sigma-Aldrich, 2006]

2.4.5 Absorbance of the Materials

In Figure 2.7 the absorbance of the different materials have been plotted. In an optimal polymer solar cell materials will not absorb light at the same wavelength as the active layer. This means that none of the materials PCBM, PEDOT:PSS and ITO can absorb light at the same wavelength as MEH-PPV. This is important because only the light absorbed by MEH-PPV may result excitons. It is seen, that PEDOT:PSS absorbs some light at the same wavelength as MEH-PPV. Therefore the PEDOT:PSS layer has to be very thin in order to minimize the absorbance.

2.5 Lifetime of Polymer Solar Cells

The stability of polymer solar cells is an important factor which must be controlled to some extent before an introduction to the commercial market can be a reality. The typical lifetime of a simple polymer solar cell (ITO/Polymer/Aluminum) in air and under illumination ($1000 W m^{-2}, AM1.5$) is a few hours, while the lifetime of inorganic solar cells is 25 years.[Krebs et al., 2005]

Before the lifetime can be improved it is necessary to understand why the polymer solar cells degenerate. This section will be used to emphasize some of the factors that influence the degeneration.

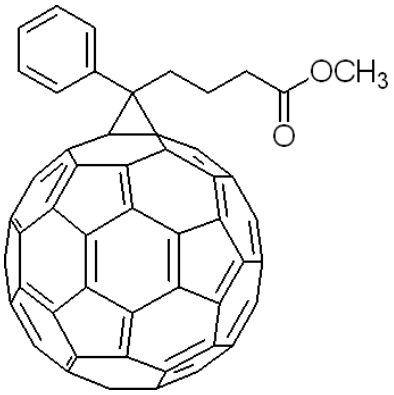

Figure 2.6: The figure shows the modified C_{60}, PCBM. The upper attachment is the one making the molecule soluble in organic solvents[Sigma-Aldrich, 2006]

Lifetime tests carried out on different types of polymer solar cells by [Krebs et al., 2005] show that the degeneration is not caused by a single factor. The degeneration occurs when the solar cells are illuminated, kept in dark, in normal atmosphere, and in vacuum.

Experiments carried out in dark and light indicate that a part of the degeneration is photo related. Degeneration occur in both cases but it happens faster when the device is illuminated. The speed of the degeneration even vary with the intensity of the light and that might indicate that there exists a link between the current density and degeneration.[Krebs et al., 2005]

Parallel test carried out in a controlled atmosphere and in vacuum have shown that the presence of oxygen is crucial for the degeneration. In the absence of oxygen the degeneration was reduced significantly and a further reduction of the degeneration speed was obtained when devices were kept in dark and vacuum. Polymer solar cells kept in dark and vacuum for 5 days showed barely any sign of degeneration.[Krebs et al., 2005]

Studies of the concentration of oxygen through the device have shown that oxygen from the atmosphere diffuse through the aluminum electrode into the active layer. The accumulation of oxygen is highest at the interface between the polymer and the aluminum layer and then drops through the active layer. It was also proven that aluminum diffuses into the polymer layer, where it reacts with molecular oxygen and creates an isolating layer.[Norrman and Krebs, 2006]

It is clear that the lifetime of polymer solar cells can be improved if an effective shielding can be made and if the diffusion of aluminum into the polymer layer can be stopped. The shielding can be done by glass and it has been reported that an introduction of a lithium fluoride (LiF) layer in between the aluminum electrode and the active layer can increase the stability of polymer solar cells.[Krebs et al., 2004]

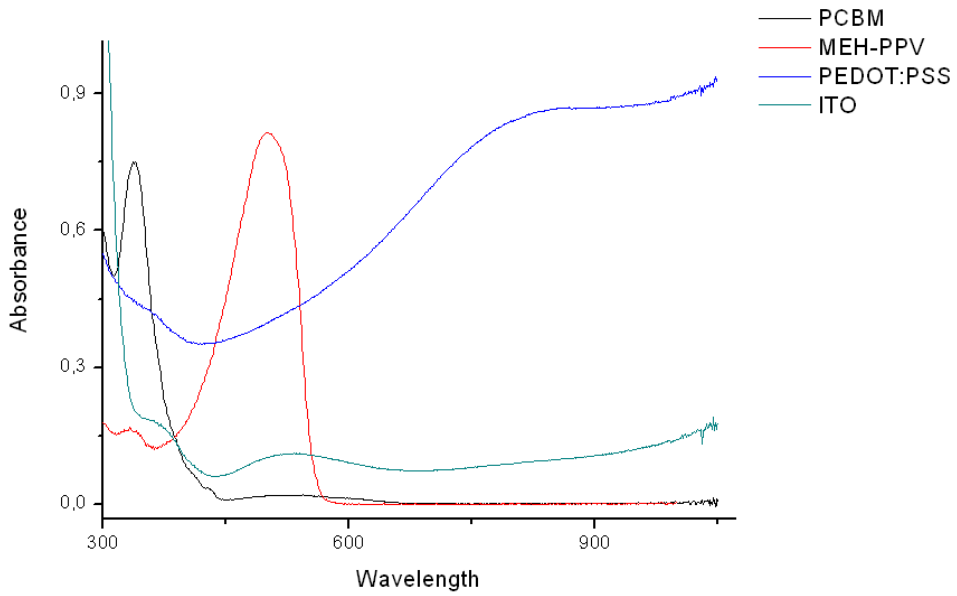

Figure 2.7: Shows the absorbance of ITO, PEDOT:PSS, MEH-PPV and PCBM

2.6 The Solar Spectrum

The output of a solar cell is dependent on the radiative spectrum and two spectra used for comparison of two solar cells must match each other very closely. Therefore a convention regarding the radiative spectrum of solar cell testing lamps must be specified. When a solar cell is in use, the radiative spectrum is that of the sun therefore the specified spectrum must resemble that of the sun.

In order to determine the shape and energy of that spectrum a certain analysis of the solar spectrum has to be done.

The sun emits radiation in the whole electromagnetic range but the intensity is concentrated close to the visible range, 300 to 800 nm. The radiation peaks in the green-blue area.

In Figure 2.8 two spectra of the sun can be seen. They are part of the reference AM 1.5 spectra produced by the American Society for Testing and Materials (ASTM) in 2003. The first spectrum is an extraterrestrial spectrum. The second spectrum is an AM 1.5 spectrum at specified atmospheric conditions, see [for Testing and (ASTM), 1999].

The total energy received can be calculated by integrating the data and is approximately $1353 Wm^{-2}$ for the extraterrestrial spectrum. When entering the atmosphere of the earth a large part of this energy is absorbed and scattered. This absorption and scattering is more evident at certain wavelengths matching the absorption and scattering spectra of the atmospheric constituents. Light below 300nm is cut off by O_2, ozone, and nitrogen. CO_2

and water is responsible for the notches at 900, 1100, 1400, 1900, 1800 and 2600nm. [Nelson, 2003]

Furthermore the spectrum in general is attenuated due to the length traveled within the atmosphere of the earth. In order to describe this a new term called airmass is introduced. The $n_{airmass}$ is given by the ratio between the diameter of the atmosphere and the actual optical path, see Equation 2.1.

$$n_{airmass} = \frac{\text{Actual optical path}}{\text{Diameter of the atmosphere}} = \csc(\gamma) \tag{2.1}$$

γ being the angle from the horizon to the sun. Eg. AM 1.5 corresponds to an angle at 42°.

The energy received at the surface of the earth is given by the integrated AM 1.5 solar spectrum, and gives 900 Wm^{-2}. However, for convenience, the AM 1.5 spectrum is normalized so that the energy received is 1000 Wm^{-2}.

In Figure 2.8 both the extraterrestrial and the airmass 1.5 solar spectrum is displayed up to a wavelength of 2000 nm. Note that around 200 Wm^{-2} is received from 2000 to 4000 nm but this part is left out for clarity of the remaining spectrum. Secondly the photon energy of this part (approx. 0.6eV at wavelength 2000 nm) is too low to excite electrons across the bandgap of the polymers and therefore uninteresting in the context of polymer solar cells. [Nelson, 2003]

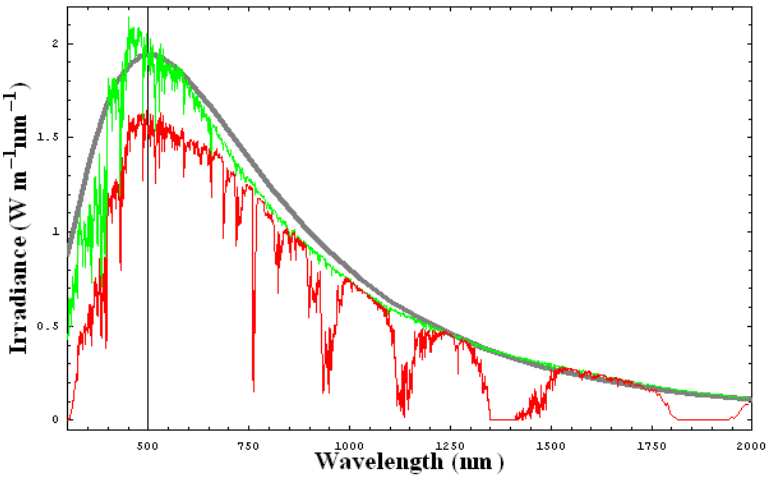

Figure 2.8: The two black curves are the extraterrestrial solar spectrum and the solar spectrum at airmass 1.5. The grey curve is the radiation from a black body at 5760° C. The data is from [for Testing and (ASTM), 1999].

When designing a lamp for testing solar cells it is very important to maintain a close relationship with the sun. The intensities at various wave-

lengths should match as closely as possible and the integrated energy must be 1000 Wm^{-2}

The extraterrestrial spectrum of the sun resembles that of a black body with temperature given by the temperature on the surface of the sun. The number of photons at a given energy is given by Equation 2.2 and is also plotted in Figure 2.8.

$$n(\omega) = \left(\frac{2}{h^3c^2}\right)\frac{E^2}{\exp\left(\frac{E}{k_BT}\right) - 1} \tag{2.2}$$

$n(\omega)$ is the number of photons at frequency ω, k_B is the Boltzmanns constant, T is the surface temperature of the sun, E is the radiative photon energy given by Planck's equation, $E = \hbar\omega$. [Nelson, 2003]

This takes no consideration of the light absorbed by different constituents in the solar nor earthly atmosphere. However the black body radiation spectrum is a good model for the spectrum of the sun and can simplify various calculations.

2.7 Project Limitation

This section will be used to outline the purpose of this project. The goal for this project can be divided into two groups: Construction of polymer solar cells and development of a program for calculating the bandstructure and absorbance spectrum of certain molecules.

Construction of polymer solar cells: Different types of the polymer/fullerene heterojunction solar cells will be made and tested. In all solar cells the active layer will be a blend between MEH-PPV and PCBM. The variations will be at the junction between electrodes and the active layer, where different concepts will be tried out. A description of the different types of polymer solar cells that will be made can be found in Section 5.1. Furthermore an ordinary silicon solar cell will be tested for comparison with the constructed polymer solar cells.

Development of a program: The purpose with this part of the project is to develop a program, which can be used to calculate energy levels, band structures, and absorbance spectra for conjugated polymers and fullerenes. This program can then be used to check if a certain polymer or fullerene has the optical properties that make them suitable in a polymer solar cell. The validity of the program will be tested by comparison of the calculated data and the experimentally obtained data.

2.8 Problem Statement

The purpose of this project was outlined in the previous section and through the construction of solar cells and through the calculations from the program, the following questions will be tried answered:

- How are changes at the electrodes reflected in the performance of the solar cells?
- How accurate can the program predict the optical properties of conjugated polymer and fullerenes?

Chapter 3

Theoretical Foundation

In order to increase the understanding of the physics in solar cells, various phenomena are given a thorough investigation in this chapter. This includes a description of the conjugated polymers in which the exciton formation occurs, the current-voltage characteristic of a solar cell, a characterization of the lamp used, excitons, and a tight-binding model for the electron structure of conjugated molecules.

3.1 Conjugated Polymers

Conjugated polymers are a group of polymers, which exhibit a variety of electronic properties. This type of polymers can have electronic conductivity ranging from insulators to conductors. Strong luminescence and strong nonlinear optical properties have also been observed from this type of polymers.

In the 1970s three scientists, Alan G. MacDiarmind, Hideki Shirakawa, and Alan J. Heeger, discovered that certain types of conjugated polymers can be chemically modified to conduct electricity. This discovery has opened a new fields of chemical and physical research, and since the 1970s conjugated polymers have attracted more and more attention form the scientific world. Scientists are now trying to find smart ways to utilize these properties in light-emitting diodes, displays for mobile telephones, flexible solar cells, and other electronic devices.[Britannica.com, 2006]

Before the properties of conjugated polymers can be fully utilized it is important to get an understanding of the structure of these polymers and their electronic properties. Therefore an introduction to conjugated polymers will be given in the following sections.

3.1.1 Bonds and Orbitals

Conjugated polymers are, like other polymers, macromolecules that consist of a long chain of repeated units called monomers. These monomers consist mostly of carbon and hydrogen atoms, but other atoms like oxygen, sulfur, and nitrogen can also be a part of the monomer, see Figure 3.1

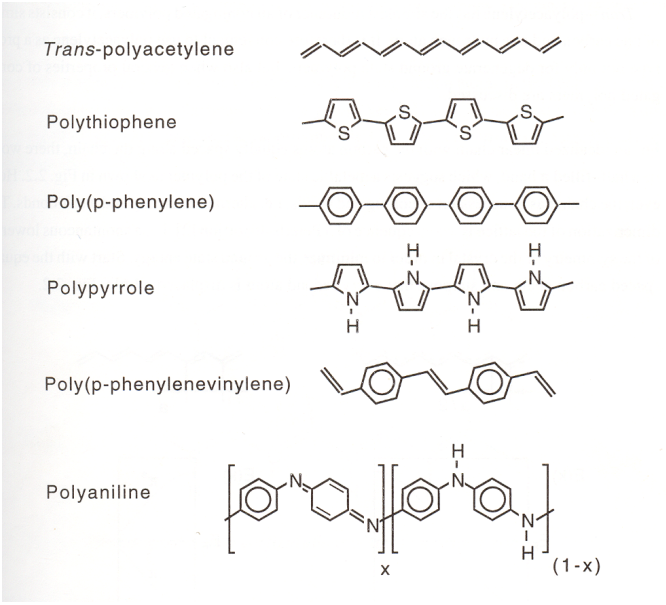

Figure 3.1: illustrates some common conjugated polymers.[Boman, 1995]

The difference between conjugated polymers and other polymers lies in the backbone of the polymers, which in the case of conjugated polymers consist of alternating single and double covalent bonds between the carbon atoms. The single bond consists of a σ bond and the double bond consists of a σ bond and a π bond. The simplest conjugated polymer is trans-polyacetylene, which is an isomer of polyacetylene, see Figure 3.1

To explain these two types of bonds it is necessary to look at the valence electrons of carbon. Every carbon atom has four valence electrons where, in the ground state configuration, a single carbon atom has two valence electrons placed in the $2s$ orbital and two valence electrons in two different $2p$ orbitals.

The sigma bonds are formed by two overlapping sp^2 orbitals, where the sp^2 orbital is a hybridization between one electron from the $2s$ orbital and the two electrons from the $2p$ orbitals. This hybridization form three in plane orbitals at angles of 120 degrees. Two of the orbitals form bonds with neighboring carbon atoms and the third one is forming a bond, away from the backbone, with a hydrogen or another atom.

The fourth valence electron is placed in a $2p$ orbital perpendicular to the plane spanned by the three other orbitals. Each electron in the $2p$ orbital along the chain interacts with a neighboring $2p$ electron and forms a π bond. The two electrons in a π bond occupy the space above and below the σ bond, as illustrated in Figure 3.2. [Boman, 1995]

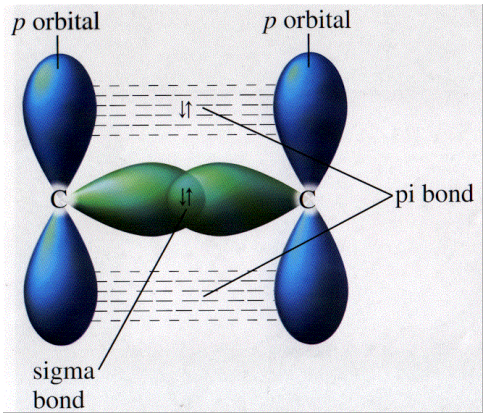

Figure 3.2: illustrates the σ and the π bonds between two carbon atoms.[Zumdahl, 2003]

3.1.2 Band Structure of Conjugated Polymers

When determining the band structure of conjugated polymers, the polymers can be divided into two classes. The first class consist of polymers that posses a degenerate ground state and the second class is polymers with a non-degenerate ground state.

Trans-polyacetylene is the simplest conjugated polymer and belongs to the class of polymers with a degenerate ground state. The monomer of trans-polyacetylene consists only of one carbon and one hydrogen atom, see Figure 3.1 Because of the simplicity, this polymer will be used to discuss the degenerate ground state.

If the carbon atoms in the chain were equally spaced, the system of $2p$-orbitals would create a half-filled π bond. This half-filled π band will result in a metallic state of the polymer as shown in Figure 3.3. However in trans-polyacetylene the chain has success with the creation of conjugated bonds i.e. altering strong and weak bonds, see Figure 3.3. These creations of altering bonds result in a non-equal spacing of the carbon atoms, where the double bonds have a length of 1.36 Å and the single bonds have a length of 1.44 Å. This change in the lattice is a consequence of a Peierls distortion, which describes a spontaneous lowering of the symmetry of the lattice in order to minimize the ground state energy. The displacement of every second atom reduces the translation symmetry and halves the first

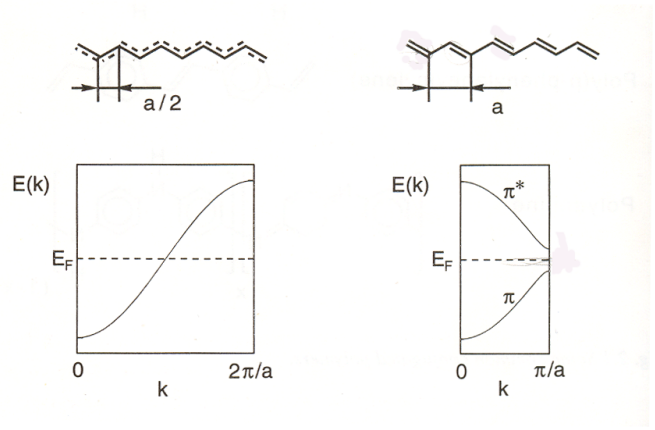

Figure 3.3: (Left) The band structure of a carbon chain with equally spaced atoms. (Right) The band structure of a carbon chain with altering single and double bonds.[Boman, 1995]

Brillouin zone. After the periodic distortion two new π bands are formed: one filled (π) and one empty (π^*). The two bands repel each other and opens up a band gap at the Brillouin zone boundary. This band gap is caused by the altering single and double bonds, which leads to a periodic perturbation of the potential.[Boman, 1995]

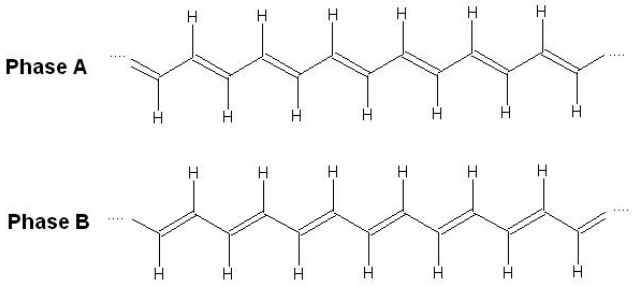

Figure 3.4: The two ground state configurations of trans-polyacethylene.

The band gap in trans-polyacetylene is about 1.8 eV at the Brillouin zone boundary. As it can be seen in Figure 3.4, can trans-polyacetylene have two ground state configurations, phase A and phase B. Phase B can be obtained from phase A by the exchange of the single and double bonds. Since all the carbon atoms are equivalent if the chain is infinite, the energies of the two phases are equal i.e. the ground state of the polymer is degenerated.

An example of a conjugated polymer with a non-degenerate ground state is polythiophene where the monomer is a thiophene. Two connected thiophene rings are illustrated in Figure 3.5. As it can be seen from the figure

the ring has two non-equivalent carbon sites. C_α connects the thiophene ring to a neighboring ring in the chain and C_β forms a bond to a hydrogen side group. The hydrogen atoms on neighboring rings repel each other, which leads to a rotation of the rings around the chain axis.

In the ground state configuration of polythiophene the neighboring C_α and C_β atoms are connected with a double bond. The C_α-C_α and the C_β-C_β are both connected with single bonds. Since the C_α and the C_β are non-equivalent an exchange of the double and single bonds along the chain will lead to state of another energy. This means the ground state of the polymer is non-degenerate.

The minimum band gap between the highest valence band and the lowest conduction band is approximately 2.0 eV.[Boman, 1995]

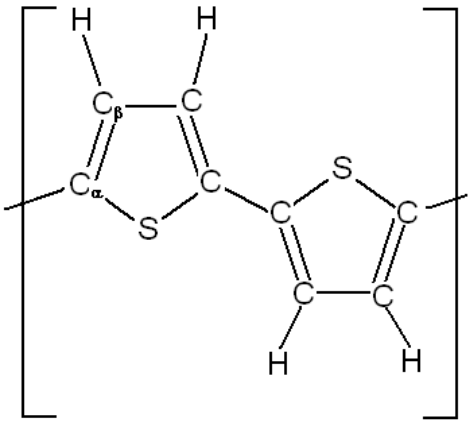

Figure 3.5: illustrates two connected thiophene rings. In the left ring is the two non-equivalent carbon sites marked with C_α and C_β.

In general the band gap of conjugated polymers lies between 1.5 and 4 eV, but the size of these band gabs can be modified chemically.[Carlberg, 1996]

3.1.3 Polarons and Bipolarons

A polaron can be formed when an electron is removed (or injected) from the neutral chain, by chemical doping. This introduced charge polarizes the surrounding chain and creates a local deformation of the lattice. The charge and the surrounding deformation are in quantum mechanics referred to as a polaron. This local deformation of the chain results in a lowering of a conducting state and a raise of a valence state and thereby moving two electronic states into the band gap.[Boman, 1995]

Depending on the type and level of doping different polarons can be created. A hole polaron is created when the polymer is p-doped i.e. an

electron has been removed form the chain. In the absence of an electron the lower level only contain one electron and the upper level is empty, see Figure 3.6. An electron polaron is formed when the polymer is n-doped i.e. an electron has been introduced into the chain. In the presence of an extra electron the lower level is filled with two electrons and the upper level has gained an electron.[Boman, 1995]

At high doping level of the polymer two polarons can recombine and form a double charged bipolaron. In a hole bipolaron the absence of two electrons result in an empty upper and lower level. The electron bipolaron has gained two electrons from the doping process and therefore both levels are filled with two electrons, see Figure 3.6.[Boman, 1995]

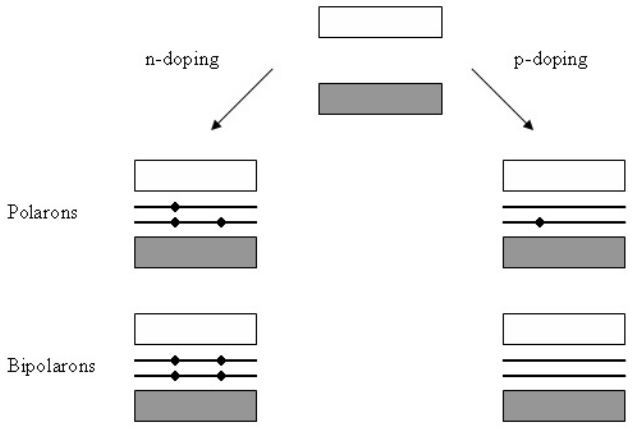

Figure 3.6: Schematic illustration of an electron polaron and bipolaron to the left and a hole polarons and bipolaron to the right.

Doping of the polymer is not the only way to create polarons. When an exciton, caused by the absorption of a photon, is dissociated into a hole and an electron two differently charged polarons are formed.[Carlberg, 1996]

3.2 Characterizing a Solar Cell

In order to characterize a solar cell a few terms must be established. These are given below and will be discussed in the following sections.

V_{oc}	The open circuit voltage.
I_{sc}	The short circuit current.
FF	The ratio between the product of the maximum current and voltage and the V_{oc} and I_{sc}
η	The efficiency of the solar cell.

3.2.1 Current Generated in a Solar Cell

An illuminated solar cell can take the place of a battery or a current generator in a simple electric circuit.

When there is no load present the current drawn through the circuit is the short circuit current, I_{sc}. When a load is present the current will be between 0 and I_{sc}, and the value is determined by the IV characteristic. The short circuit current is given by Equation 3.1.

$$I_{sc} = \int QE(E)n(\omega)dE \tag{3.1}$$

$n(\omega)$ is the solar flux of photons with energy $E = \hbar\omega$ and $QE(E)$ is the quantum efficiency. $QE(E)$ is a material constant and is defined as the probability for an incident photon to generate an electron at the external circuit. Generally, $QE(E)$ depends on the parameters of the solar cell, that is, the absorption coefficient, the efficiency of charge separation and the efficiency of charge collection etc. It does not depend on the incident spectrum though.[Nelson, 2003]

3.2.2 Dark Current

A diode admits much larger current when a voltage is applied in one direction, forward bias, than in the other, reverse bias. A solar cell is acting as a diode under bias, and the current generated by this bias is called dark current. The current will flow in the opposite direction of the photocurrent canceling the net current.

The potential difference can be a result of an applied bias but potential difference will also build when the solar cell is connected in an electrical circuit with a load.

$$I_{dark}(V) = I_0(\exp\frac{qV}{k_BT} - 1) \tag{3.2}$$

I_0 is a constant for the given solar cell, V is the applied voltage, T is the temperature, q is the elementary charge, and k_B is Boltzmann's constant.

The overall current of the solar cell as a function of the applied voltage is called the current voltage characteristic and can be approximated as the sum of the short circuit and dark current. This is only valid for an ideal diode and is given by Equation 3.3.

$$I(V) = I_{sc} - I_{dark}(V) = I_{sc} - I_0(\exp\frac{qV}{k_BT} - 1) \tag{3.3}$$

At some voltage the dark current will negate the photocurrent and the net current will be zero. This voltage is called the open circuit voltage V_{oc}.

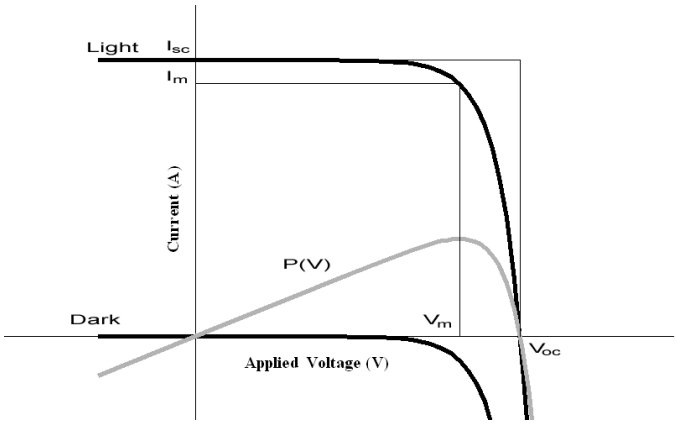

Figure 3.7: A simulated IV characteristic. The IV curve in dark and in light is shown along with the power as a function of the applied voltage. The point of maximum power is indicated along with I_{sc} and V_{oc}

From Equation 3.3 the open circuit voltage can be derived and is given in Equation 3.4.

$$V_{oc} = \frac{k_B T}{q} \log(\frac{I_{sc}}{I_0} + 1) \tag{3.4}$$

In an electric circuit the solar cell is equivalent to a parallel connected current generator with a diode. This is displayed in Figure 3.8. When a voltage is applied the current will be divided between the load and the diode. As the voltage increases the diode will allow more current to pass yielding a maximum level of voltage. In Figure 3.7 an IV curve is displayed. [Nelson, 2003]

3.2.3 Efficiency

The power generated by a solar cell at a given voltage is given by Equation 3.5.

$$P = IV \tag{3.5}$$

Note that the solar cell can operate at a voltage only between 0 and V_{oc}. The power will increase with increasing voltage until a maximum is reached at V_m and I_m and then drop to zero at V_{oc}. This is described by the fill factor, FF, which is defined in Equation 3.6

$$FF = \frac{V_m I_m}{V_{oc} I_{sc}} \tag{3.6}$$

The FF is a measure of how much voltage relative to V_{oc} the cell can deliver without a significant loss of current.[Nelson, 2003]

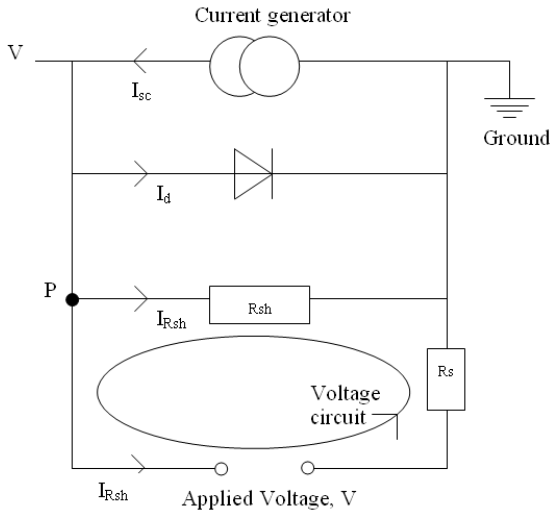

Figure 3.8: An electrical circuit equivalent with a solar cell using a current generator including the parasitic resistances simulating the power loss at the contacts and from leakage current. The series connected resistance, R_s, is simulating a resistance in the electrode-polymer interface. The shunt resistance R_{sh} simulates a leakage around the polymer layer between the two electrodes. Furthermore the point P and a voltage circuit are emphasized as they are basis for the calculation of the current generated by the solar cell.

For an applied voltage above V_{oc} the solar cell consumes power, and with increasing voltage some solar cells may start function as a diode and emit light.

3.2.4 Parasitic Resistance

In practice power will flow through leakage currents around the cell and be lost in the contacts. These flaws can be simulated with two parasitic resistances. To describe the power lost in leakage currents running around the polymer layer between the contacts, a parallel connected or shunt resistance, R_{sh} is introduced. For power lost in resistance at the interface between the electrodes and within the electrodes, a series resistance R_s is introduced. See Figure 3.8.

In order to describe the current generated at a given applied voltage it is necessary to calculate the currents and voltages in the circuits. This can be described with $V = IR$ and Kirchoffs laws. The current is evaluated at a point P and the voltage drop around the marked circuit and the circuit with the diode and applied voltage is used to set up the equations of 3.7.

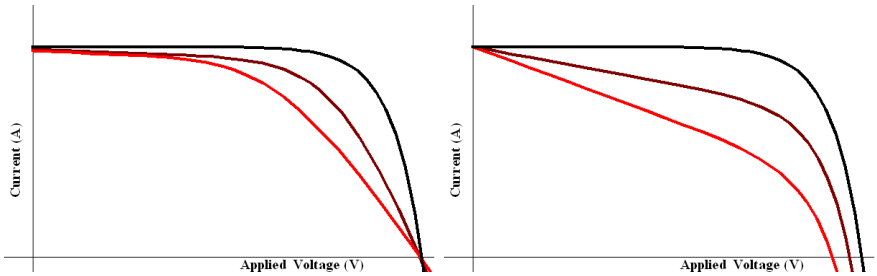

Figure 3.9: Here the effect from the parasitic resistances are shown. The black curve is in both graphs displayed for $R_s = 0$ and $R_{sh} = \infty$. To the left the effect of a series resitance is shown with increasing series resistance. To the right the effect of a decreasing shunt resistance is shown.

$$I_{sc} - I_d = I_{R_{sh}} + I_{R_s} \tag{3.7}$$
$$V + V_{R_s} = V_{R_{sh}} \tag{3.8}$$
$$V + V_{R_s} = V_d \tag{3.9}$$

From combining the equations of 3.7 an expression for the current as a function of the applied voltage can be achieved. It is given in Equation 3.10.

$$I(V) = \frac{(I_{sc} - I_0(\exp{(\frac{q(V - I(V)R_s)}{k_B T}}) - 1))R_{sh} - V}{R_s + R_{sh}} \tag{3.10}$$

The effect of the parasitic resistances on the IV characteristic is shown in Figure 3.9. It is evident that these simulated flaws will yield a decrease in the fillfactor and thereby the efficiency of the solar cell.[Nelson, 2003]

3.2.5 Effect of Bandgap on Efficiency

An important value when comparing solar cells is the efficiency - the ratio between the incoming radiative energy and the output of electric energy. However there is a theoretical limit to this ratio.

The calculations of this section will be under the approximation that there is no recombination, there can not be multiple excitons per photon and every photon with energy $E > E_g$ generates an electron to the external circuit. Furthermore the results is only valid for a radiation source with a spectrum similar to that of a black body at temperature 5760 K as different spectra will effect both the maximum efficiency and the optimal size of bandgap.

The only part of the spectrum usable is those photons with sufficient energy to excite across the bandgap of the solar cell. However, an electron

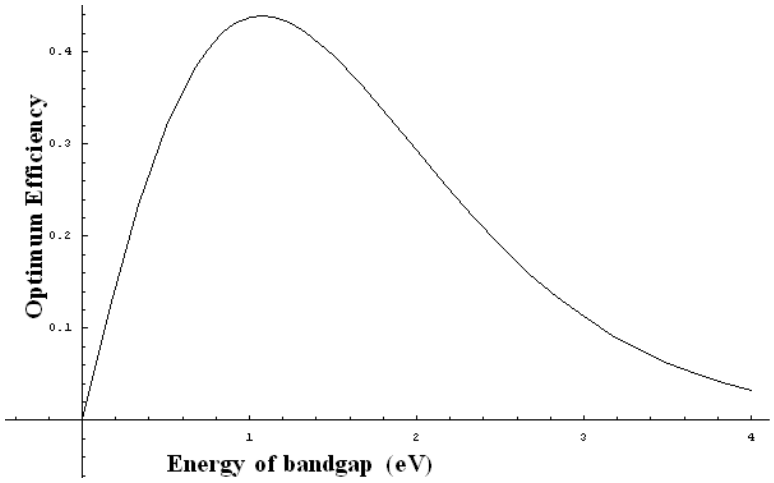

Figure 3.10: The optimal efficiency as a function of the bandgap. The optimal bandgap is calculated to be at 1.06 eV with an efficiency at 44%.

with excess energy after excitation will go trough a radiative-free transition to the lowest state of the conducting band. Therefore the ratio is dependent of the bandgap, and the optimal bandgap is determined by the equilibrium between a high energy per photon contra a high amount of exciting photons.

Using the black body radiation model of the sun, the efficiency as a function of the band gap is given by Equation 3.11.

$$\Phi(E_g) = \frac{E_g \int_{E_g}^{\infty} n(\omega) d\omega}{\int_0^{\infty} n(\omega) \hbar\omega d\omega} \tag{3.11}$$

Φ being the theoretical utilization ratio and E_g is the energy of the bandgap and $n(\omega)$ is the black body photon flux at energy $\hbar\omega$.

The utilization ratio as a function of the energy of the bandgap is plotted in Figure 3.10.

The optimal bandgap can be found by solving Equation 3.12. For the black body spectrum used for this analysis the optimal bandgap gives 1.06 eV yielding an efficiency at 44%.

$$\frac{d\Phi}{dE_g} = 0 \tag{3.12}$$

3.3 The Spectrum of the Lamp

In Section 2.6 the spectrum of the sun was described. As already mentioned the solar cells must be designed for working with sunlight, light with the spectral characteristic and intensity as that from the sun. It is however for practical reasons standart to use a lamp radiating $1000 W m^{-2}$.

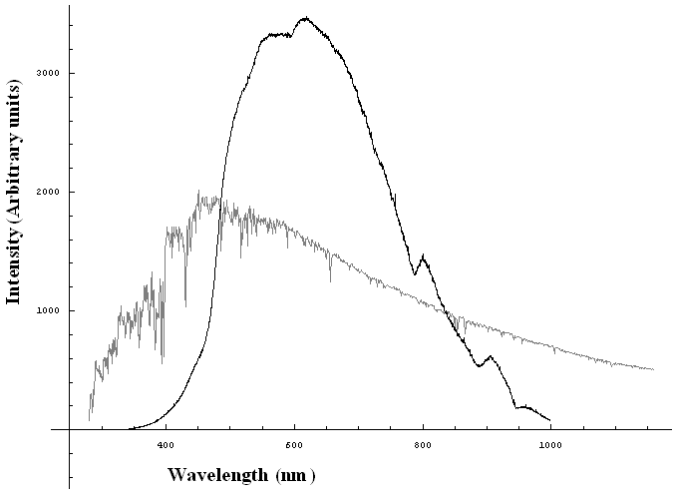

Figure 3.11: The spectrum of the lamp (the black curve) compared with the spectrum of the sun(grey curve). Note that the spectra are normalized with regard to the integrated energy for better comparison.

In Figure 3.11 the spectrum of the lamp used for measuring IV characteristics is shown along with the AM1.5 spectrum of the sun for comparison. Note that the spectra are normalized so that the integrated energy output is equal.

As clarified in Section 3.2.5 it is only photons with an energy higher than the bandgap that are of use. Therefore the integrated energy from E_g to infinity for a given lamp should be equal to that of the sun in order for the lamp and the sun to result in a similar exciton generation.

It is evident from Figure 3.11 that the solar spectrum is much wider, peaking blueshifted compared to the lamp. Furthermore the light intensity from the lamp is centered around 500nm. The differences in spectrum must be taken into consideration when comparing efficiency of different bandgap solar cells.

The bandgap of a silicon solar cell is approximately 1.4 eV corresponding to a wavelength at around 850nm. The bandgap of a polymer solar cell is generally higher, and using MEH-PPV as the active layer the bandgap is around 2.14 eV corresponding to 580 nm [Chambers and Selmic, 2005]. Consequently the ratio between the energy the silicon solar cell and the MEH-PPV solar cell will be able to utilize is a relatively larger using the lamp than the sun.

The quality of the lamp is sufficient for the measurements conducted in this project. However a different lamp should be used in order to increase the validity of the IV characteristics and efficiency measurement.

3.4 Generation and Dissociation of Excitons

This section describes the principles behind generation and separation of photo generated excitons in crystals. The principles described here applies to the excitons generated in polymer solar cells as well. Excitons are the basic for the photocurrent, and they are the key parameter to efficient solar energy conversion. Therefore, a good understanding of the nature of excitons is needed in order to make efficient solar cells.

3.4.1 Excitons in Crystals

When a crystal is illuminated with photons $\hbar\omega > E_g$ electrons are excited to higher energy levels by absorbance of a photon. An excited electron leaves behind an empty space, and this empty space is termed a hole. The hole acts as if it was a positively charged electron, it can move through the crystal and it is affected by coulomb forces. Therefore, a coulomb potential exists between the excited electron and the positively charged hole. This potential acts to bind the pair together, so that they cannot be easily separated. The electron hole pair is called an exciton. An exciton is similar to a hydrogen atom, the hole being the positively charged core.[Kittel, 2005]

Generally, when a photon of energy $\hbar\omega > E_g$ is absorbed in a crystal an electron is excited to a higher energy level. This means that the crystal only absorbs the photon frequencies corresponding to an energy equal to or higher than the band gap. But some materials absorb photons with energies lower than the band gap. This is the case with solid krypton, which has a band gap of 11.7 eV but shows an absorbtion peak at 10.17 eV. This is due to the generation of excitons. The energy levels of excitons generally lies below the band gap, allowing for absorbtion of photons with lower energy. [Kittel, 2005]

An exciton can move in a crystal and transport energy because the electron-hole pair carries momentum and thus, kinetic energy. The exciton cannot, however, carry a current because it is electrically neutral. For a photovoltaic cell to work, free charge carriers have to be present. Since the electrons in a semiconductor are too tightly bound to contribute to the current, only the excited electron and the hole can make a contribution. This implies that the electron has to be separated from the hole.[Kittel, 2005]

3.4.2 Dissociation of Excitons

As noted in the last section, it is necessary to separate the bound electron hole pair to create free charge carriers. This separation can be achieved by applying an electric field across the exciton. This will pull the electron and the hole in opposite directions and thus enable transport of charge. The electron hole transport process is illustrated in Figure 3.12.

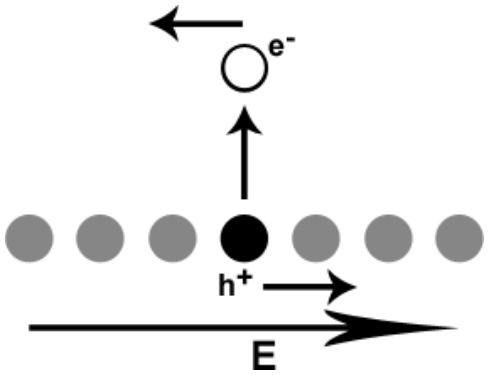

Figure 3.12: An illustration of the excitation of an electron to a higher energy level, and the separation of the pair by an electric field.

One of the most important factors in making good solar cells, is efficient dissociation of excitons. Even if all incident light is absorbed in the cell, it contributes nothing to the performance of the cell if the dissociation process is inefficient. The effectiveness of dissociation is dependent on the strength of the applied electric field. The stronger the field, the faster the electron hole pair is pulled from each other, decreasing recombination frequency. Types of electron hole recombination events include radiative recombination and Auger recombination. Radiative recombination happens when an electron undergoes spontaneous emission, crosses the band gap and emits a photon with frequency $\omega = E_g/\hbar$.

3.4.3 Calculation of Exciton Binding Energy

The effectiveness of charge separation depends on the binding energy of the excitons. An approximated calculation of the binding energy of excitons in PPV is given in this section. The exciton binding energy can be calculated by considering the Rydberg energy. The Rydberg energy is derived for an hydrogen atom, but since an exciton is comparable to a hydrogen atom, the Rydberg energy can be applied to excitons as well. The energy of the electron in the hydrogen atom is dependant on the coulomb interaction and the kinetic energy of the electron.

$$E = \frac{1}{2} m_e v^2 - \frac{1}{4\pi\epsilon_0} \frac{e^2}{r} \tag{3.13}$$

Where r is the radius of orbit. By considering the forces acting on the electron an expression for the speed of the electron can be obtained. The electron is subject to the coulomb force and to an acceleration due to the circular orbit. From Newtons 2nd law an expression for the velocity can be derived.

$$\frac{m_e v^2}{r} = \frac{1}{4\pi\epsilon_0}\frac{e^2}{r^2} \tag{3.14}$$

Thus we find:

$$v^2 = \frac{1}{4\pi\epsilon_0}\frac{e^2}{m_e r} \tag{3.15}$$

Inserting this result in Equation 3.13 gives the following expression for the energy:

$$E = \frac{1}{8\pi\epsilon_0}\frac{e^2}{r} - \frac{1}{4\pi\epsilon_0}\frac{e^2}{r} \tag{3.16}$$

Gathering the terms we obtain an expression for the energy of the electron:

$$E_R = \frac{-1}{8\pi\epsilon_0}\frac{e^2}{r} \tag{3.17}$$

This expression is called the Rydberg energy. In the case where r is equal to a_0, the Bohr radius, E_R equals $-13.6eV$ which is the ionization energy for the hydrogen atom. In the case of excitons, r is not equal to the Bohr radius but is calculated from Equation 3.18. Furthermore, the permittivity is not the vacuum permittivity ϵ_0 but the permittivity of the material in which the excitons are generated.

$$r = \frac{4\pi\epsilon_0\epsilon_r\hbar^2}{e^2\mu} \tag{3.18}$$

Here ϵ_r is the relative permittivity of MEH-PPV and μ is the reduced mass. The permittivity $\epsilon_0\epsilon_r$ is used to account for the screening of the coulomb potential by attracted electrons and holes. This permittivity should also be used when calculating the Rydberg energy of the exciton. It should be noted that the permittivity used is the *macroscopic* permittivity. This means that the approximation is only valid when the radius of the exciton is large in comparison to the lattice constant.

The reduced mass which is used in the calculation of the exciton binding radius can be calculated from Equation 3.19.

$$\mu = \frac{m_e^* m_h^*}{m_h^* + m_e^*} \tag{3.19}$$

Where * means effective mass. The effective mass can be described as follows. When an electron is inside a material, it experiences interactions with the material. This means that the acceleration due to a force F is not determined solely by the electron mass m_e but also by the interactions from the material. These interactions can be included in the mass so that $F = m_e^* \frac{dv}{dt}$, where m^* is the effective mass and $\frac{dv}{dt}$ is the acceleration of the electron in the material due to the force F. An expression for the effective mass can be derived using the definition of force and acceleration, and the group velocity for the electron wave packet.

$$F = \frac{dp}{dt} = \hbar \frac{dk}{dt} \tag{3.20}$$

$$a = \frac{dv}{dt} = \frac{dv}{dk}\frac{dk}{dt} \tag{3.21}$$

Inserting in Newton's second law

$$\hbar \frac{dk}{dt} = m^* \frac{dv}{dk}\frac{dk}{dt} \tag{3.22}$$

Using the group velocity $v_g = \frac{d\omega}{dk}$ and $\omega\hbar = E$ we get:

$$m^* = \hbar^2 \left(\frac{d^2 E}{dk^2} \right)^{-1} \tag{3.23}$$

This expression shows that the effective mass is inversely proportional to the curvature of the band structure. If the band structure is known the exciton binding energy can be calculated using first Equation 3.23 to find the effective mass for electrons and for holes, and then using Equation 3.17 to calculate the binding energy.

3.4.4 Determination of Dissociation Efficiency

The efficiency of dissociation is in general dependant on the electric field applied to across the exciton. The stronger the field, the faster the electron-hole pair will be pulled apart, and the less time is available for recombination. The recombination event is relatively slow, in the order of μs [Nelson, 2003] . Dissociation efficiency is as noted earlier also dependant on the exciton binding energy, this energy was calculated in the previous section.

The exciton is held together by the energy from the attractive coulomb force, this energy should be overcome by the energy put into the exciton by the field. The energy due to the coulomb attraction is given by $E_c = \frac{-1}{4\pi\epsilon_0\epsilon_r}\frac{e^2}{r}$ and the energy due to the electric field is given by Equation 3.24.

$$E_E = -eEx_h + eEx_e \tag{3.24}$$

Here E is the field strength, x_e is the electron position and x_h is the hole position. This calculation can be intuitively understood by considering the potential energy of the electron and the hole due to the field. This scenario is illustrated in Figure 3.13.

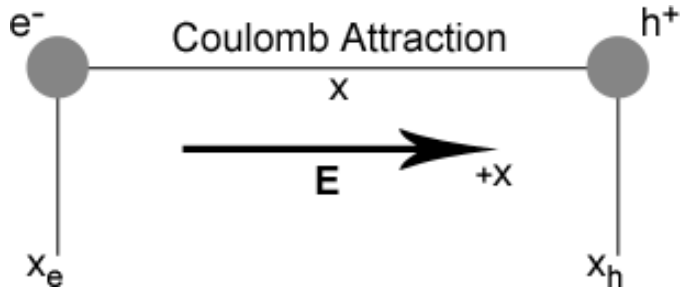

Figure 3.13: The electron and the hole at positions x_e and x_h respectively. The electric field is directed along the positive x-axis. The separation between the electron and the hole is x.

The field works to increase the x-position of the hole and decrease the x-position of the electron. When x_h is increased or x_e decreased, the potential energy of the system drops. This explains the signs in Equation 3.24. According to Figure 3.13 $x = x_h - x_e$, using this, Equation 3.24 is rewritten to $E_E = -eEx$. Using this along with the potential energy of the exciton due to the coulomb attraction gives the following expression for the energy as a function of the electron position relative to the hole position x:

$$E(x) = \frac{-1}{4\pi\epsilon_0\epsilon_r}\frac{e^2}{|x|} - eEx \tag{3.25}$$

Here the numerical value of x is used in the first term because the coulomb potential energy is only dependant on the absolute distance between the charges. The potential energy from the field however, is strongly dependant on the sign of the separation. Moving the electron far right and the hole far left in Figure 3.13 would reverse the sign of the separation and increase the potential energy. This increase would not be reflected in the calculation if the numerical value of x was used in the last term.

If the graph of E versus x is plotted a graph similar to the one in Figure 3.14 is obtained. The graph goes to minus infinity as $x \to 0$ due to the term E_c. When x becomes smaller than zero the energy rises. This corresponds to the electron and the hole interchanging their positions and working against the field, and this of course increases the energy.

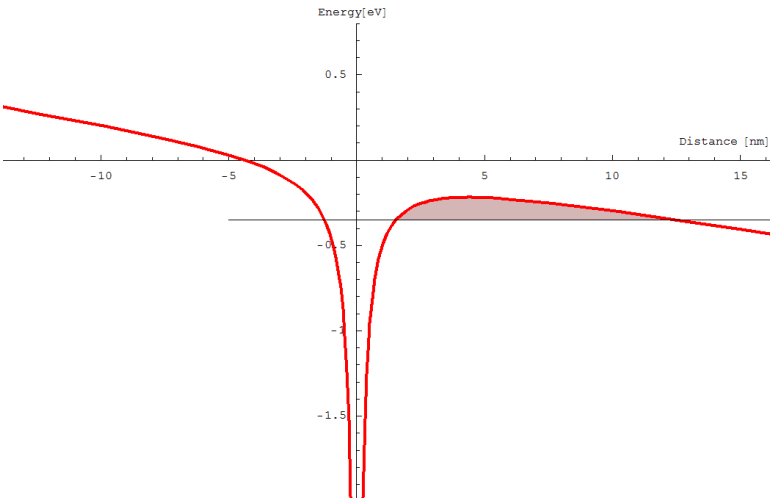

Figure 3.14: Graph showing the binding energy of the exciton under an applied electric field and the potential barrier which the electron has to overcome to separate from the hole. The tunneling probability increases when the area of the shaded area decreases.

When x is positive the energy is first increasing due to the coulomb attraction being stronger than the electric field force. When the separation reaches a certain limit, the electric field force is stronger than the attraction and separation continues because it lowers the energy.

From the graph it can be seen that the exciton has to cross an energy barrier to dissociate. The black line in the figure represents the energy of the exciton when it is created. This energy can be calculated from Equation 3.18 and Equation 3.17. If this energy is smaller than the barrier, the electron (or hole) has a certain probability to tunnel through the barrier to increase the separation. The tunneling probability is dependent on the area bounded by the line and the curve (the shaded area in the figure). The smaller the area, the larger the probability. When C_60 is added to the solar cell the binding energy decreases and the black line moves against zero decreasing the area of the shaded area.

3.4.5 Tunneling Through the Barrier

As noted in the previous section the electrons has to tunnel through a potential barrier to separate from the holes. The probability of tunneling (transmission) is given by the Wentzel-Kramer-Brillouin (WKB) formula, Equation 3.26:

$$T(E) = T_0 Exp\left\{-2\int_{x_i}^{x_f}\sqrt{\frac{2m}{\hbar^2}\left(V_B(x) - E\right)}dx\right\} \tag{3.26}$$

Here $V_B(x)$ is the barrier energy as a function of the separation x, m is the mass of the tunneling particle and T_0 is the tunneling probability when the energy is larger the barrier height.

The potential barrier over which the integration is done is shown in Figure 3.14, and the integration limits are marked with the black line. The position of the line on the y-axis represents the binding energy of the exciton. When the binding energy increases the barrier width increases drastically. Furthermore, the difference $V_B(x) - E$ gets larger because the barrier height increases as well. The overall result is that the exponent gets larger, and the tunneling probability decreases accordingly.

The integration limits are found by equating Equation 3.25 to the binding energy and finding the intersections. Because we are interested only in the points of intersection for which x is positive, $|x| = x$ and the equation can be rewritten to a second degree polynomial. The lower root of this polynomial is x_i and the higher root is x_f.

The tunneling probability as a function of the binding energy can be seen in Figure 3.15. The relative permittivity of MEH-PPV used is $\epsilon_r = 3.0$ [Yang et al., 2000]. The exciton binding energy in PPV has been measured to 0.35 eV [Alvarado et al., 1998], this gives a probability for exciton dissociation of about 0.75. In Figure 3.16 and Figure 3.17 the tunneling probability as a function of applied field is shown. The binding energy was set to 0.35 eV.

In Figure 3.15 it is seen that the tunneling probability increases as the binding energy decreases. This is expected because the height of the barrier decreases. It can be seen that the probability eventually reaches unity, this happens when the binding energy becomes equal to the height of the potential barrier. In Figure 3.17 the tunneling probability as a function of field strength is plotted. Again, the probability increases as the field strength increases as expected.

3.5 Tight Binding Approximation

In this project the tight binding (TB) method is utilized to calculate the energy eigenvalues and band structure of the polymers and of C_{60}. TB is an approximation which simplifies the calculations significantly. In molecules even as simple as H_2 the Hamiltonian contains as many as 8 terms, two for the kinetic energy of the electron and the proton, and 6 for the potential energy of the electrostatic interactions between pairs of electrons and protons.

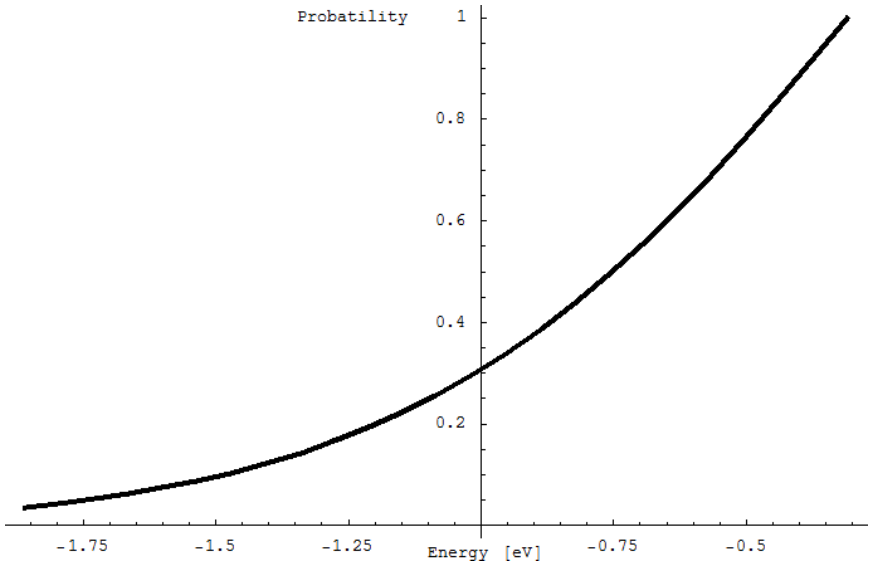

Figure 3.15: The probability of tunneling as a function of exciton binding energy. Higher energy (numerically) means lower probability. The field strength was set to $2.5 \times 10^7 [V/cm]$.

Calculating the energy levels of C_{60} using an exact model would be practically impossible. Therefore some approximations are made. The TB model is based on the idea that complicated molecular wave functions, can be build from simple atomic wave functions (linear combination of atomic orbitals, LCAO). The molecular wave function ψ is written as a linear combination of atomic time independent wave functions [Lewars, 2004], [Kittel, 2005]:

$$\psi = \sum_{i=1}^{N} \sum_{\alpha=1}^{n} c_{i\alpha} \phi_{i\alpha} \tag{3.27}$$

The first summation runs over the number of atoms in the solid, and the second summation runs over the number of orbitals in every atom. In the case of planar polymers we are only considering π orbitals because the electrons in π orbitals are the most loosely bound electrons. The summation is therefore rewritten into:

$$\psi = \sum_{i=1}^{N} c_i \phi_i \tag{3.28}$$

Where the ϕ_i's are now the atomic π orbitals. This wave function is not an exact solution to the Shrödinger equation for the system, only an

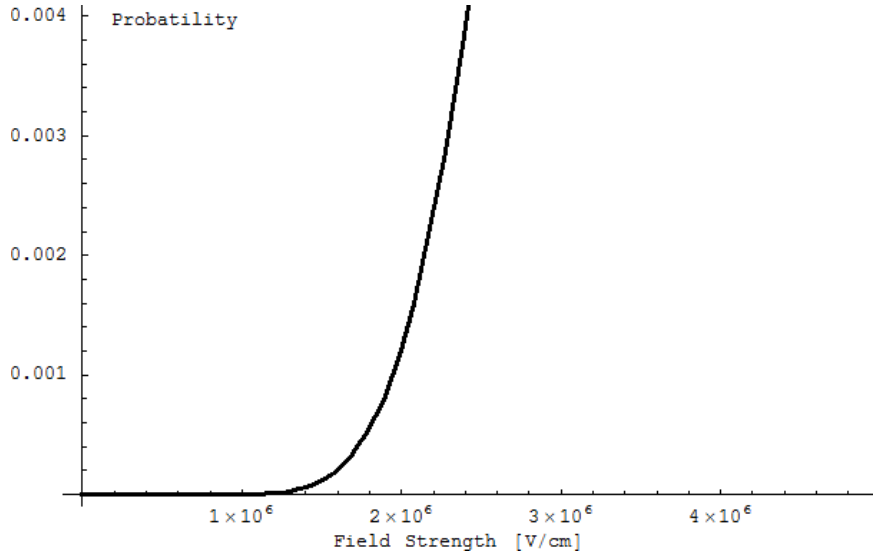

Figure 3.16: Probability as a function of field strength, the exciton binding energy is set to $-0.35eV$*. This field strength is shown in the interval* 0 *to* 4×10^6

approximated solution. We want to make this approximation as good as possible. The variational principle states that the expectation value of the energy for a trial wavefunction, is always greater than or equal to the ground state energy. The expectation value is calculated using:

$$< \psi|\hat{H}|\psi >= \frac{\int \psi^* \hat{H} \psi d^3r}{\int \psi^* \psi d^3r} \tag{3.29}$$

Now, as stated before, according to the variational principle:

$$\frac{\int \psi^* \hat{H} \psi d^3r}{\int \psi^* \psi d^3r} \geq E_0 \tag{3.30}$$

Because it is guaranteed that the energy of the trial wave function will always be greater than or equal to the true ground state energy, we are free to choose the c_i's which minimizes the expectation value of the energy. The closer the expectation value gets to the ground state energy, the more accurate the approximation is.

For simplicity we will consider a two atom system where only two orbitals are allowed to interact. The results obtained using this simplification can easily be expanded to systems of larger numbers of orbitals. Using Equation 3.28 a two atomic system implies that $\psi = (c_1\phi_1 + c_2\phi_2)$. Inserting this in Equation 3.30, assuming that the wave-function is entirely real , gives:

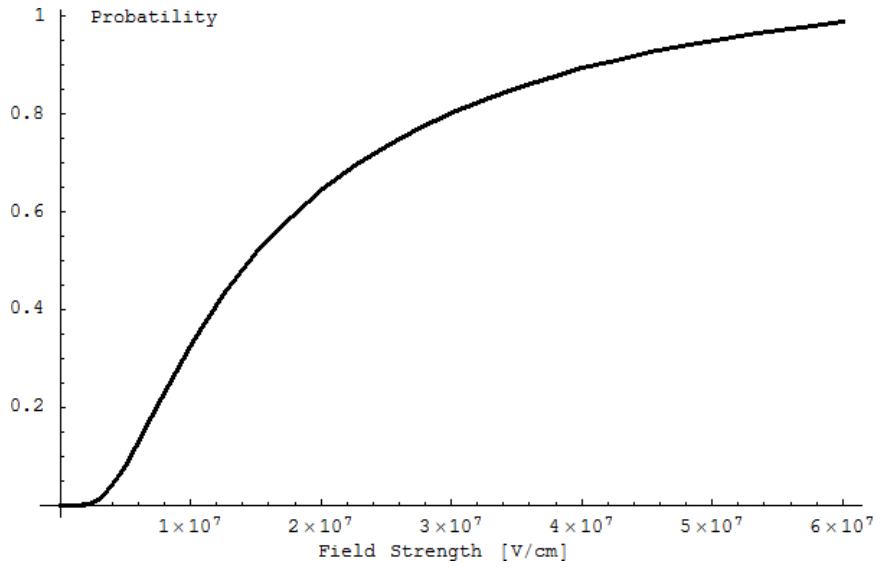

Figure 3.17: Probability as a function of field strength, the exciton binding energy is set to $-0.35eV$. This field strength is shown in the interval 0 *to* 6×10^7

$$\frac{\int (c_1\phi_1 + c_2\phi_2)\, \hat{H}\, (c_1\phi_1 + c_2\phi_2)\, d^3r}{\int (c_1\phi_1 + c_2\phi_2)^2} \geq E_0 \tag{3.31}$$

Now, looking only at the nominator and expanding the parentheses:

$$c_1^2 \int \phi_1 \hat{H} \phi_1 d^3r + c_1c_2 \int \phi_1 \hat{H} \phi_2 d^3r + c_1c_2 \int \phi_2 \hat{H} \phi_1 d^3r + c_2^2 \int \phi_2 \hat{H} \phi_2 d^3r \tag{3.32}$$

The first of these integrals is called the coulomb integral (only the integral, not the constants c_x). It is a measure of the energy of an electron in atomic orbital one. This integral is from now on denoted as α_i. The two middle integrals are called resonance integrals. They are a measure of the strength of bonding as a result of overlap of atomic orbital one and two, they are denoted as β_{ij}. The last integral is equivalent to the first one. Now looking at the denominator of Equation 3.31:

$$c_1^2 \int \phi_1^2 d^3r + c_1c_2 \int \phi_1\phi_2 d^3r + c_1c_2 \int \phi_1\phi_2 d^3r + c_2^2 \int \phi_2^2 d^3r \tag{3.33}$$

The first and the last integrals are equal to 1 because the wave function is normalized, and integration is done over all space. The two middle integrals

are termed overlap integrals, and they are a measure of the efficiency of the overlapping of the wave functions. The overlap integral is denoted as S_{ij}.

The physical significance of the integrals α, β and S can be explained as follows. α_i is the energy of the molecule relative to zero, where zero energy is defined as the energy of the molecule when the electron is at an infinite distance from the orbital. Because the energy of the molecule decreases as the electron falls into the orbital, α_i is a negative value. The negative of α_i is equal to the ionization energy, it is the energy needed to remove an electron from the orbital to a point infinitely far away.

β_{ij} is a measure of the strength of the bond between overlapping orbitals. It can be viewed as the energy of an electron in the overlap region of the orbitals. β_{ij} is a negative value.

The S_{ij} integral is a measure of the efficiency of overlap of atomic orbitals. It is less than one between different atomic orbitals on the same atom, and between separated atomic orbitals. Between identical orbitals on the same atom $S = 1$ because the wave function is normalized. When two atoms are far separated from each other the overlap integral is effectively equal to zero. Figure 3.18 illustrates the overlapping wave functions.

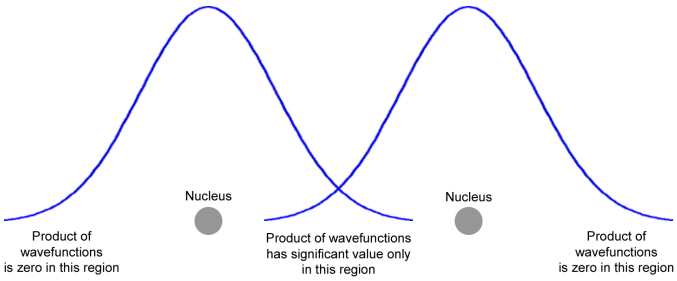

Figure 3.18: An illustration of the overlap of wave functions. The overlap integral has a significant value only in the region between neighboring atoms, because the product of the wavefunction is close to zero elsewhere.

Introducing α, β and S in Equation 3.32 and Equation 3.33 we get the following:

$$E = \frac{c_1^2\alpha_1 + c_2^2\alpha_2 + 2c_1c_2\beta_{12}}{c_1^2S_{11} + c_2^2S_{22} + 2c_1c_2S_{12}} \tag{3.34}$$

Where the fact that the Hamiltonian is a hermitian operator, and β_{ij} therefore equals β_{ji}, has been used. The next step is to minimize the energy by choosing the c_i's which gives the smallest possible energy. This is done by differentiating the energy function first with respect to c_1 and then with respect to c_2 and setting the derivatives $\frac{\partial E}{\partial c_1}$ and $\frac{\partial E}{\partial c_2}$ equal to zero. Doing this the following equations are obtained:

$$0 = c_1 (\alpha_1 - ES_{11}) + c_2 (\beta_{12} - ES_{12}) \tag{3.35}$$
$$0 = c_1 (\beta_{21} - ES_{21}) + c_2 (\alpha_2 - ES_{22}) \tag{3.36}$$

These equations are called the secular equations. The resemblance to a matrix problem is obvious. The indices correspond to the row and column where they lie (α_i lies at i, i). Rewriting these equations into a matrix problem:

$$\begin{pmatrix} \alpha_1 - ES_{11} & \beta_{12} - ES_{12} \\ \beta_{21} - ES_{21} & \alpha_2 - ES_{22} \end{pmatrix} \cdot \begin{pmatrix} c_1 \\ c_2 \end{pmatrix} = \begin{pmatrix} 0 \\ 0 \end{pmatrix} \tag{3.37}$$

By noting that we are everywhere subtracting some scalar quantity times the scalar E, this matrix problem can be rewritten into:

$$[\mathbf{H} - \mathbf{S}E] \cdot \mathbf{c} = \mathbf{0} \tag{3.38}$$

Where the **H** and **S** matrices look as follows:

$$\mathbf{H} = \begin{pmatrix} \alpha_1 & \beta_{12} \\ \beta_{21} & \alpha_2 \end{pmatrix}, \quad \mathbf{S} = \begin{pmatrix} S_{11} & S_{12} \\ S_{21} & S_{22} \end{pmatrix} \tag{3.39}$$

The **H** matrix is called the *Fock* matrix, and it represents the energy of the system. These matrices are further simplified using the Hückel approximation which is described in the next section.

3.5.1 The Simple Hückel Approximation

In the simple Hückel approximation, overlapping between atomic orbitals is neglected, meaning that S_{ij} equals zero for $i \neq j$. Only perfect overlap between identical orbitals on the same atom is considered, corresponding to $S_{ii} = 1$. A matrix element can be expressed as $S_{ij} = \delta_{ij}$, where δ_{ij} is Kronecker delta. This means that the overlap matrix **S** will be of the form:

$$\mathbf{S} = \begin{pmatrix} 1 & \cdots & 0 \\ \vdots & \ddots & \vdots \\ 0 & \cdots & 1 \end{pmatrix} \tag{3.40}$$

Or in other words, the matrix **S** will be equal to the unit matrix **I**. Using this Equation 3.41 is rewritten into:

$$[\mathbf{H} - \mathbf{I}E]\,\mathbf{c} = \mathbf{0} \tag{3.41}$$

The generalized eigenvalue problem Equation 3.41 has been rewritten into the normal eigenvalue problem because $\mathbf{S} = \mathbf{I}$. Non trivial solutions to this equation exists only when the determinant of $[\mathbf{H} - \mathbf{I}E]$ is equal to zero. Finding the values of E for which this is true, corresponds to finding the eigenvalues of the matrix $\mathbf{H}$.

In the simple Hückel approximation the matrix $\mathbf{H}$ is a hermitian matrix with the diagonal elements α_{ii}'s equal to zero. α_{ii}'s different from zero will only shift the energy values by a constant value . The β_{ij}'s are set equal to some constant value representing the binding energy on adjacent atoms, and zero when the atoms are not adjacent. By doing this, interaction between non-neighbor atoms are neglected.

3.5.2 Tight Binding for Benzene

As an example of the use of tight binding a benzene molecule will be considered. Benzene is a planer molecule with the π orbitals oriented perpendicular to the molecule plane. A picture of benzene if shown in Figure 3.19.

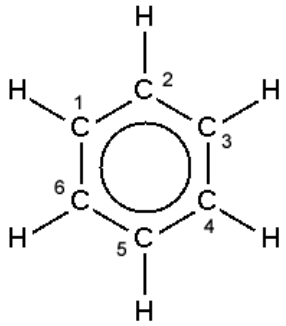

Figure 3.19: A benzene molecule with numbered carbon atoms.

Building the $\mathbf{H}$ matrix is done by considering interactions between atoms. As noted earlier, in the simple Hückel approximation only interactions between adjacent atoms are considered. For benzene, the $\mathbf{H}$ matrix is a 6x6 matrix, because there are 6 carbon atoms in benzene, and it looks as follows:

$$\mathbf{H} = \begin{pmatrix} 0 & \beta & 0 & 0 & 0 & \beta \\ \beta & 0 & \beta & 0 & 0 & 0 \\ 0 & \beta & 0 & \beta & 0 & 0 \\ 0 & 0 & \beta & 0 & \beta & 0 \\ 0 & 0 & 0 & \beta & 0 & \beta \\ \beta & 0 & 0 & 0 & \beta & 0 \end{pmatrix} \tag{3.42}$$

The β's at position $(6,1)$ and $(1,6)$ is due to interactions between atom 1 and 6.

3.5.3 Tight Binding for Polymers - Bloch Theorem

In polymers there are an infinite number of interactions between atoms. This means that the matrices will be of infinite dimension. Like in a crystal, the energy levels will split into bands when free atoms are brought together [Kittel, 2005]. To calculate the energy bands of the polymer, the Bloch theorem is used. According to the Bloch theorem the wavefunction can be written as the product of a plane wave and a periodic function $u(\mathbf{r})$, which has the periodicity of the lattice [Kittel, 2005]:

$$\psi\left(\mathbf{r}\right) = e^{i\mathbf{k}\cdot\mathbf{r}} u\left(\mathbf{r}\right) \tag{3.43}$$

Because $u(\mathbf{r})$ is periodic $u(\mathbf{r}) = u(\mathbf{r}+\mathbf{T})$, where $\mathbf{T}$ is a translation vector of the lattice. The only change in moving from one unit cell to another is an extra factor of e^{ika}. This can be seen from Equation 3.44:

$$\psi\left(\mathbf{r}+\mathbf{a}\right) = e^{i\mathbf{k}\cdot(\mathbf{r}+\mathbf{a})} u\left(\mathbf{r}\right) = e^{i\mathbf{k}\cdot\mathbf{r}} e^{i\mathbf{k}\cdot\mathbf{a}} u(\mathbf{r}) \tag{3.44}$$

Because $u(\mathbf{r}+\mathbf{a}) = u(\mathbf{r})$. The tight binding matrices used for crystals and polymers contain interactions from neighboring unit cells as well as interactions between atoms in the molecule. As an example of a tight binding matrix using the Bloch theorem, we will consider polyacetylene as shown in Figure 3.20.

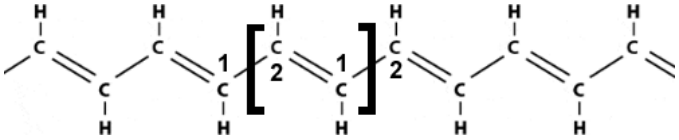

Figure 3.20: Polyacetylene.

The tight binding matrix for polyacetylene is a 2×2 matrix since there are two atoms in the unit cell. The unit cell is marked with brackets in the figure, and the atoms are numbered. To obtain the elements of the matrix the definitions of α and β are used, as well as the Bloch theorem. The interaction of orbital π_2 with all π_1 orbitals in the polymer is given by:

$$H_{12} = \sum_n e^{ikan} \int \pi_1(\mathbf{r}+n\mathbf{a}) \hat{H} \pi_2(\mathbf{r}) d^3r \tag{3.45}$$

Similarly, the interaction of orbital π_1 with all π_2 orbitals is given by:

$$H_{21} = \sum_n e^{ikan} \int \pi_2(\mathbf{r} + n\mathbf{a}) \hat{H} \pi_1(\mathbf{r}) d^3r \tag{3.46}$$

Where the summation runs over all the unit cells in the polymer. For infinite polymers this would mean $n = [-\infty, +\infty]$, but in the Hückel approximation only nearest neighbor interactions are considered so $n = [-1, 0, 1]$. The equations are thus rewritten to:

$$H_{12} = e^{-ika} \int \pi_1(\mathbf{r} - \mathbf{a}) \hat{H} \pi_2(\mathbf{r}) d^3r + \int \pi_1(\mathbf{r}) \hat{H} \pi_2(\mathbf{r}) d^3r + e^{ika} \int \pi_1(\mathbf{r} + \mathbf{a}) \hat{H} \pi_2(\mathbf{r}) d^3r \tag{3.47}$$

$$H_{21} = e^{-ika} \int \pi_2(\mathbf{r} - \mathbf{a}) \hat{H} \pi_1(\mathbf{r}) d^3r + \int \pi_2(\mathbf{r}) \hat{H} \pi_1(\mathbf{r}) d^3r + e^{ika} \int \pi_2(\mathbf{r} + \mathbf{a}) \hat{H} \pi_1(\mathbf{r}) d^3r \tag{3.48}$$

In Equation 3.47 the first integral corresponds to interaction between atom two in the marked unit cell and atom 1 in the unit cell to the left. These are connected by a single bond. The second integral is the interaction between atom 2 and 1 in the same unit cell, they are connected by a double bond. The last integral is interaction between atom 2 in the marked unit cell and atom 1 in the next unit cell to the right, but since these atoms are not nearest neighbors, this integral equals 0. Using a similar procedure in Equation 3.48 the we get:

$$H_{12} = \beta_D + \beta_S e^{-ika} \tag{3.49}$$

$$H_{21} = \beta_D + \beta_S e^{ika} \tag{3.50}$$

Using $H_{ii} = \alpha$ as derived earlier, the $\mathbf{H}$ matrix for poly acetylene is given by:

$$\mathbf{H} = \begin{pmatrix} \alpha & \beta_D + \beta_S e^{-ika} \\ \beta_D + \beta_S e^{ika} & \alpha \end{pmatrix} \tag{3.51}$$

By varying the values of k through the first Brilluoin zone and calculating the energy eigenvalues for each k the band structure is obtained. This procedure is explained in Chapter 4.

Chapter 4

Software - EBCalc

This chapter describes the functionality of the program EBCalc - Energy Band Calculator. EBCalc is a piece of software able to calculate the energy bands of various molecules. In the context of polymer solar cells, it is used to calculate the band structure of the polymer and C_{60}.

EBCalc is written purely in C++ using the Windows GDI (Graphics Device Interface) of the Win32 API. It is targeted for WindowsXP or Windows2000 machines. The program makes use of a mathematics library which has been created by this project group, and optimized in interest of reusability. The library is implemented through a number of C++ classes. These classes implements functionality like complex number algebra, vector and matrix algebra, plotting of functions and drawing of coordinate systems, numerical integration and differentiation etc.

The actual implementation of these classes will not be discussed, only the Jacobi method is described in detail because it plays such an important role.

The theoretical results which were calculated using the program are presented in the last section of this chapter.

4.1 Finding Eigenvalues by Jacobi Transformations

To calculate the energy levels of the polymer the equations from quantum mechanics have to be solved. This involves solving the energy eigenvalue problem for the system. This eigenvalue problem has the form of Equation 4.1.

$$\hat{H}\psi = E\psi \tag{4.1}$$

To solve this problem, we have to find the eigenvalues E which satisfies the above equation. The equation is first rewritten into a matrix problem,

this process is explained in Section 3.5. Equation 4.2 shows the eigenvalue problem on matrix form.

$$\mathbf{H} \cdot \mathbf{c} = E\mathbf{S} \cdot \mathbf{c} \tag{4.2}$$

Finding eigenvalues is not a trivial task, in fact it is one of the most difficult tasks in numerical computation. A routine for finding eigenvalues of a general matrix would both be very complicated, and very slow. Therefore eigenvalue routines are often highly specialized, utilizing certain properties of the matrices involved. One such specialization is based on Jacobi Transformations. This routine can be used when the matrices involved are equal to the transpose of their conjugate. Such matrices are called hermitian matrices. The hermitian of a matrix is denoted $A^\dagger$ so for hermitian matrices $A^\dagger = A$. The following sections describes the basics of the Jacobi algorithm.

4.1.1 What is the Jacobi Method

The aim of the Jacobi method is to create a diagonal matrix through a series of similarity transformations. These similarity transformations are plane rotations, designed to annihilate (set to zero) an off diagonal matrix element on each rotation. The similarity transformations are of the form shown in Equation 4.3.

$$\mathbf{D} = \mathbf{V}^T \cdot \mathbf{A} \cdot \mathbf{V} \tag{4.3}$$

where,

$$\mathbf{V} = \mathbf{P}_1 \cdot \mathbf{P}_2 \cdot \mathbf{P}_3 ...$$

Here the $\mathbf{P}_i$'s are the successive Jacobi rotation matrices, and $\mathbf{D}$ is the final diagonalized matrix. Because similarity transformations do not change the eigenvalues of a matrix, and because the eigenvalues of a diagonalized matrix, are the diagonal elements themselves, the diagonal of the matrix $\mathbf{D}$ are the eigenvalues of $\mathbf{A}$.

Furthermore, because the matrix which diagonalizes $\mathbf{A}$ is the matrix of the eigenvectors, the eigenvectors can be calculated by multiplying the successive transformations.

4.1.2 The Jacobi Rotation Matrix

The Jacobi rotation matrix is of the form seen in Equation 4.4. The matrix is termed $\mathbf{P}_{pq}$ because it is the matrix which is designed to annihilate matrix element p, q. It has a cosine at p, p and q, q and a sine and a -sine at q, p

and p, q respectively. In this section cosine is termed c, sine is termed s and tangent is termed t.

$$\mathbf{P}_{qp} = \begin{pmatrix} 1_{11} & & & & & & \\ & \cdots & & & & & \\ & & c_{pp} & \cdots & s_{pq} & & \\ & & \vdots & 1 & \vdots & & \\ & & -s_{qp} & \cdots & c_{qq} & & \\ & & & & & \cdots & \\ & & & & & & 1_{nn} \end{pmatrix} \tag{4.4}$$

In one Jacobi iteration p and q are varied so as to annihilate every element of the matrix. Because successive transformations in the same iteration undo previously set zeros, more than one iteration is needed, but the convergence of the transformations guarantee that the result will eventually be a diagonal matrix. A Jacobi transformation is shown in Equation 4.5

$$\mathbf{A}' = \mathbf{P}_{pq}^T \cdot \mathbf{A} \cdot \mathbf{P}_{pq} \tag{4.5}$$

Here the matrix $\mathbf{A}'$ is the matrix obtained from a single transformation. Multiplying out Equation 4.5 and utilizing the symmetry of the matrix, the equations Equation 4.6 - Equation 4.10 are obtained.

$$a'_{rp} = ca_{rp} - sa_{rq} \tag{4.6}$$
$$a'_{rq} = ca_{rq} + sa_{rp} \tag{4.7}$$
$$a'_{pp} = c^2 a_{pp} + s^2 a_{qq} - 2sca_{pq} \tag{4.8}$$
$$a'_{qq} = s^2 a_{pp} + c^2 a_{qq} + 2sca_{pq} \tag{4.9}$$
$$a'_{pq} = \left(c^2 - s^2\right) a_{pq} + sc\left(a_{pp} - a_{qq}\right) \tag{4.10}$$

Here the lower case a's denote an element of the matrix $\mathbf{A}$ and the subscripts denote the position of the element. a'_{rp} and a'_{rq} are the elements in column r and q excluding the elements at the diagonal and the elements at q, p and p, q so $r \neq q$ and $r \neq p$. Because the goal of the Jacobi transformation is to set off diagonal elements equal to zero, a'_{pq} is set equal to zero and Equation 4.10 is rewritten into:

$$\left(c^2 - s^2\right) a_{pq} = -sc\left(a_{pp} - a_{qq}\right) \tag{4.11}$$

Gathering cosine and sine terms on one side, and a terms on the other, the following equation is obtained:

$$\frac{c^2 - s^2}{sc} = \frac{a_{qq} - a_{pp}}{a_{pq}} \tag{4.12}$$

Using the identity $\cot 2\phi = \frac{\cos^2 - \sin^2}{2\cos\sin}$:

$$\cot 2\phi = \frac{c^2 - s^2}{2sc} = \frac{a_{qq} - a_{pp}}{2a_{pq}} \tag{4.13}$$

Where ϕ is the rotation angle which annihilates element pq and qp. Using this formula it is possible to calculate the actual numerical value of the angle, and insert this value into the cosines and sines of the Jacobi rotation matrix. This however, would involve evaluating firstly an inverse trigonometric function, $\operatorname{arccot}\phi$ and secondly the sines and cosines of the angle. This is computationally expensive, and susceptive to accuracy errors. Therefore the sines and cosines of the angle are computed, and not the angle itself. [Press et al., 2002]

4.1.3 Calculation of Sines and Cosines

By using Equation 4.13 an expression for the tangent as a function of $\cot 2\phi$ can be obtained. This derivation is shown here. First Equation 4.13 is rewritten to:

$$\cot 2\phi = \frac{1}{2t} - \frac{t}{2} \tag{4.14}$$

Where the fraction on the right hand side has first been split into two terms and rewritten using $t = s/c$. All terms are gathered on the left hand side, and the resulting equation is multiplied by $2t$ giving us:

$$t^2 + 2t\cot 2\phi - 1 = 0 \tag{4.15}$$

Using the quadratic formula with the discriminant in the denominator, t can be expressed in terms of $\cot 2\phi$. This gives:

$$t = \frac{\operatorname{sign}(\cot 2\phi)}{|\cot 2\phi| + \sqrt{\cot^2 2\phi + 1}} \tag{4.16}$$

We now have an expression for tangent. Using this an expression for cosine can be derived in terms of tangent using the Pythagorean formula for tangents and secants:

$$c^2 + s^2 = 1 \tag{4.17}$$

Dividing through by c^2:

$$1 + t^2 = \sec^2 \tag{4.18}$$

Using this an expression for cosine can be obtained directly:

$$c = \frac{1}{\sqrt{t^2+1}} \tag{4.19}$$
$$s = tc \tag{4.20}$$

Since $t = s/c$. Using these equations the sines and cosines can be calculated directly, without calculating the rotation angle.[Press et al., 2002]

4.1.4 Optimizations

When the cosines and sines have been calculated, they can be inserted into the Jacobi matrix and the diagonalized matrix of eigenvalues can be obtained by doing a number of successive Jacobi rotations. This would mean that Equation 4.3 would have to be invoked a large number of times. Matrix multiplication is a slow process on a computer because it involves a lot of multiplications. Multiplying two $n \times n$ matrices involves n^3 multiplications. Because this step is the computationally most expensive in the Jacobi routine it is worth optimizing. Analyzing Equation 4.3 it can be seen that only row and column p and q are affected by the transformation. This of course implies that computing only the affected elements can greatly improve speeds. In fact, the number of multiplications per rotation is reduced from n^3 to $8n$ (excluding multiplications used in calculations of sine and cosine).

Lastly, the stop criteria for the Jacobi routine should be noted. The routine stops when the sum of the off-diagonal elements becomes equal to zero. Of course this will only happen if an infinite number of rotations are performed. But since a computer can only do calculation with finite precision, there is no need to go further than machine precision. Therefore the routine stops when the sum of the off-diagonal elements is zero to machine precision.

4.2 From a Complex to a Real Matrix

The tight-binding matrices obtained using the Bloch theorem are complex matrices. The Jacobi method implemented in the program is not well suited for complex matrices, so a method for transforming the matrix into a real matrix is used. Starting with the matrix eigenvalue problem which has to be solved:

$$\mathbf{Hc} = E\mathbf{c} \tag{4.21}$$

Now splitting the equation into it's real and imaginary parts using $\mathbf{H} = \mathbf{H_R} + i\mathbf{H_I}$ and $\mathbf{c} = \mathbf{c_R} + i\mathbf{c_I}$:

$$(\mathbf{H_R} + i\mathbf{H_I})(\mathbf{c_R} + i\mathbf{c_I}) = E(\mathbf{c_R} + i\mathbf{c_I}) \tag{4.22}$$

Multiplying out the parentheses and splitting the equation into two equations, one for the real part and one for the imaginary part gives the following matrix eigenvalue problem:

$$\begin{pmatrix} \mathbf{H_R} & -\mathbf{H_I} \\ \mathbf{H_I} & \mathbf{H_R} \end{pmatrix} \begin{pmatrix} \mathbf{c_R} \\ \mathbf{c_I} \end{pmatrix} = E \begin{pmatrix} \mathbf{c_R} \\ \mathbf{c_I} \end{pmatrix} \tag{4.23}$$

The matrix in Equation 4.23 is four times as big as the original matrix, but its elements are all entirely real valued. Furthermore, the matrix is hermitian if the original matrix is hermitian. The number of eigenvalues in the new matrix is twice the number of eigenvalues in the original matrix, but it turns out that the number of distinct eigenvalues is the same.

4.3 Constructing the TB Matrices

This section describes the construction of the tight binding matrices used for computing the band structures and the energy levels. First the construction of the TB matrix for MEH-PPV is shown. When constructing the matrix only the PPV chain is considered and not the MEH group. A PPV monomer with numbered atoms is shown in Figure 4.1

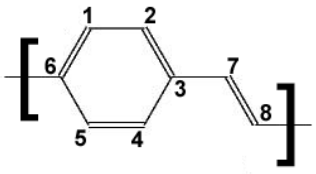

Figure 4.1: PPV with numbered atoms

Atom 8 interact with atom 6 in the next unit cell through a single bond. Therefore an extra factor of e^{ika} is introduced at matrix element $[8, 6]$ and e^{-ika} at element $[6, 8]$. The matrix used for the calculations is:

$$\begin{pmatrix} \alpha & \beta_D & 0 & 0 & 0 & \beta_S & 0 & 0 \\ \beta_D & \alpha & \beta_S & 0 & 0 & 0 & 0 & 0 \\ 0 & \beta_S & \alpha & \beta_D & 0 & 0 & \beta_S & 0 \\ 0 & 0 & \beta_D & \alpha & \beta_S & 0 & 0 & 0 \\ 0 & 0 & 0 & \beta_S & \alpha & \beta_D & 0 & 0 \\ \beta_S & 0 & 0 & 0 & \beta_D & \alpha & \beta_S & \beta_S e^{-ika} \\ 0 & 0 & \beta_S & 0 & 0 & \beta_S & \alpha & \beta_D \\ 0 & 0 & 0 & 0 & 0 & \beta_S e^{ika} & \beta_D & \alpha \end{pmatrix} \tag{4.24}$$

β_S and β_D symbolize single and double bonds respectively. This matrix is then rewritten to a real matrix using the procedure described in Section 4.2.

4.4 Using the Program

This section describes how the program is used in practice. The program supports calculation of energy levels of planar molecules like PPV and C_{60}. Strictly speaking C_{60} is not a planar molecule, but it is close enough for the program to calculate the energy levels to a good approximation. The energy levels are calculated by first loading the .xyz file of the molecule by selecting "File → Load File". In the dialog that appears, an .xyz file is selected. Only .xyz files are supported, and the program is very strict about the format of the file. The first line has to be the number of atoms in the molecule. The second line should be the name of the molecule, this line cannot be omitted! The rest of the file should be the actual data in the following format:

Format: *Atom Type* *X-Coord* *Y-Coord* *Z-Coord* *Newline*

The fields should be separated by spaces. When a file has been loaded the energy values can be calculated by selecting "Calculations → Energy Levels". The energy values are not plotted in the program, but the values can be saved to a file by selecting "Files → Save File".

Band structures can be calculated by choosing "Calculations → Energy Bands". One of the predefined polymers can be chosen, this means that the band structures calculated are not affected by the file which has been loaded. Loading a file only affects calculation of energy levels.

The **H** matrices corresponding to the chosen polymer is hardcoded into the program, but the program will do the eigenvalue calculations when a polymer has been selected. This will take a few seconds depending on the polymer chosen. When calculations has ended the band structure is plotted in the window. Band structure data can be saved to a file in the same

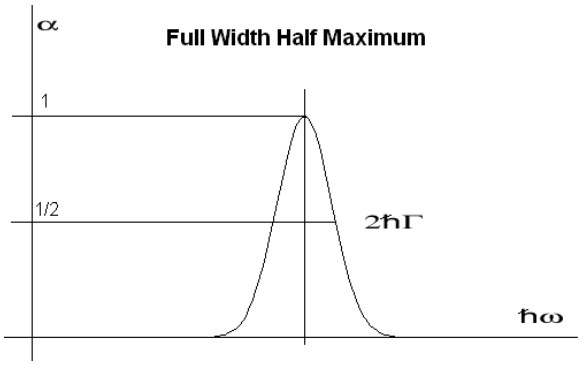

Figure 4.2: An illustration of the Full Width Half Maximum factor.

manner as saving the energy levels. Energy levels and band structure data are saved to the same file.

Lastly, if "Calculations → Exciton Field/Coulomb" is selected, the program draws the curve describing the relationship between the coulomb attraction between holes and electrons and applied field strength. The field strength can be varied by pressing the up/down keys.

4.5 Calculation of the Absorbance Spectra

The purpose of this section is to clarify the calculation of the absorbance spectrum. However the derivation of the primary equation used is beyond the scope of this project and will not be performed. Therefore the main topic here is the approximations used and the application of the equation to the present situation.

In order to calculate the absorbance it is not sufficient to simply expect very sharp absorbance lines corresponding to differences in energy levels. There are two main points that has to be taken into consideration:

Firstly not every transition between energy levels is allowed. A factor called the dipole matrix element is introduced to describe which transitions that are allowed and their probability.

Secondly, the solution contains a very large amount of molecules each with a minuscule difference in surroundings giving rise to small variations in the difference between energy levels. In order to describe this, an approximation called full width half maximum is introduced. This factor must be determined by measurements and describes the width of the peaks in the absorbance spectrum. See Figure 4.2 for an illustration of the two factors.

The equation for calculating the absorbance spectrum is given by Equation 4.25.

$$\alpha(\omega) = \frac{1}{3}(\alpha_x(\omega) + \alpha_y(\omega) + \alpha_z(\omega)) \tag{4.25}$$

The total absorbance is calculated as the sum of the absorbance of x, y, and z polarized light. The expression for the absorbance of x polarized light is given in Equation 4.26.

$$\alpha_x(\omega) = k \sum_{nocc,munocc} \frac{(\hbar\Gamma)^2 |X_{nm}|^2}{(E_{nm} - \hbar\omega)^2 + (\hbar\Gamma)^2} \tag{4.26}$$

where k is a constant which is dependent on the number of molecules per volume, $\hbar\Gamma$ is a value for the full width half maximum of peaks, X_{nm} is the dipole matrix element and is dependent on the direction under evaluation, $E_{nm} = E_m - E_n$ is the energy difference between the m'th and the n'th energy state and $\hbar\omega$ is the energy of the incident photon.

The dipole matrix element is given in Equation 4.27.

$$X_{nm} = \int \psi_n^* x \psi_m d^3r \tag{4.27}$$

where ψ_n is the molecular wavefunction with the n'th energy level of the molecule and x is an operator for the position. For x polarized light the operator equals difference in x-coordinate between a reference and the atom under evaluation. In the tight-binding approximation of Section 3.5 it was stated that the molecular wavefunction can be approximated as a sum of atomic wavefunctions or orbitals, see Equation 4.28.

$$\psi_n(\mathbf{r}) = \sum c_\alpha^{(n)} \pi_\alpha(\mathbf{r}) \tag{4.28}$$

where c_α^n is the α'th element of the n'th eigenvector.

In order to ease the calculation of the integral, a very rough approximation is applied given by Equation 4.29.

$$\int \pi_\alpha(\mathbf{r}) x \pi_\beta(\mathbf{r}) d^3r = \begin{cases} \int \pi_\alpha(\mathbf{r})^2 x d^3r & \text{for} \quad \alpha = \beta \\ 0 & \text{else} \end{cases} \tag{4.29}$$

Thereby Equation 4.30 yields for the dipole matrix element.

$$X_{nm} = \sum_\alpha c_\alpha^n c_\alpha^m \int (\pi_\alpha(\mathbf{r}))^2 x d^3r \tag{4.30}$$

To evaluate the integral of Equation 4.30 it is useful to split it in two and consider Figure 4.3.

$$\int (\pi_\alpha(\mathbf{r}))^2 x d^3r = \int (\pi_\alpha(\mathbf{r}))^2 (x - x_\alpha) d^3r + \int (\pi_\alpha(\mathbf{r}))^2 x_\alpha d^3r \tag{4.31}$$

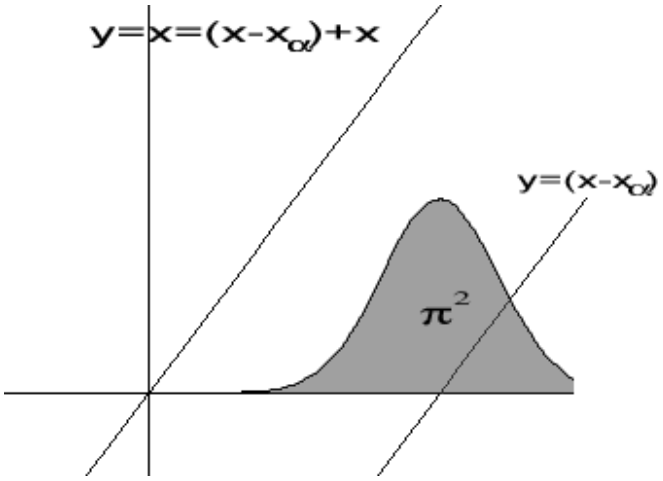

Figure 4.3: The integrand under evaluation is $x\pi^2 = (x - x_\alpha)\pi^2 + x_\alpha\pi^2$. The first integrand is an odd function while the second is the π-orbital times a constant, x_α.

The product of the squared π orbital and the $x - x_\alpha$ will always be an odd function, hence the first integral of Equation 4.31 will always equal zero. x_α is a constant under integration and due to normalization, the second integral equals x_α.

Therefore Equation 4.32 yields for the matrix dipole element.

$$X_{nm} = \sum_{\alpha} c_\alpha^{(n)} c_\alpha^{(m)} x_\alpha \tag{4.32}$$

Equation 4.32 is the summation of the dot product between the n'th and m'th eigenvector over all the atoms of the molecule under evaluation. Note that the expression is independent of the chosen point of reference as the eigenvectors per definition are orthogonal.

Thereby every term of Equation 4.26 has been clarified allowing the calculation of theoretical absorbance spectra.

4.6 Results from Theoretical Calculations

This section presents the theoretical results obtained from the calculations by the program. The band structure of PPV and PPP has been calculated using the infinite model, they are shown in Figure 4.5 and Figure 4.4. The calculated band gap of PPV is approximately 2.8 eV and the band gap of PPP is 1.0 eV indicating that they are both semiconductors.

The absorbance spectrum of C60 and PPV has been calculated used the theory described in Section 4.5. The calculated spectra are shown in Figure 4.6 and Figure 4.7.

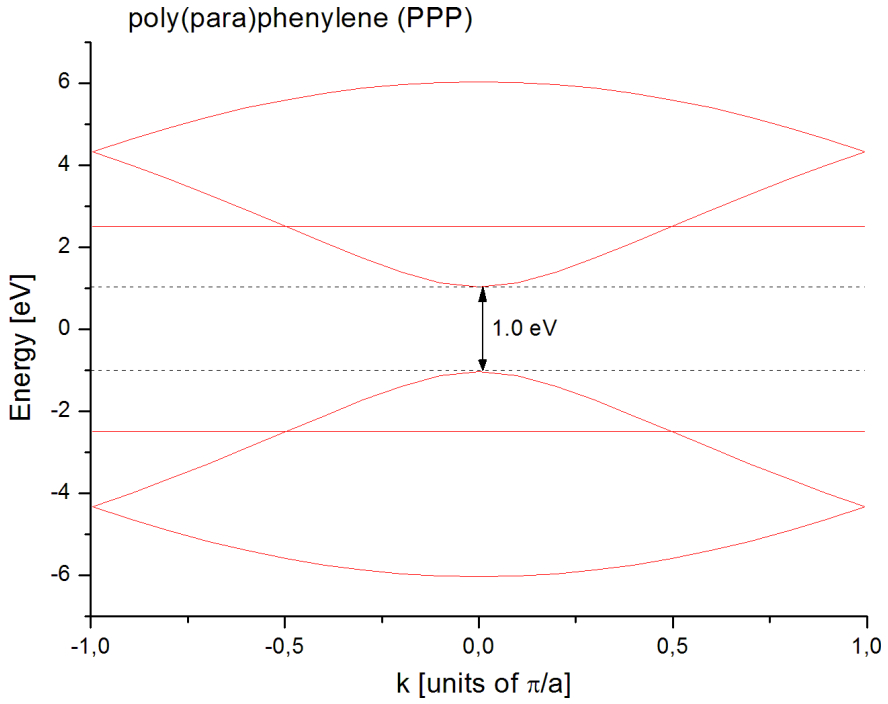

Figure 4.4: The band structure of PPP. The bands are calculated using a lattice constant of 1

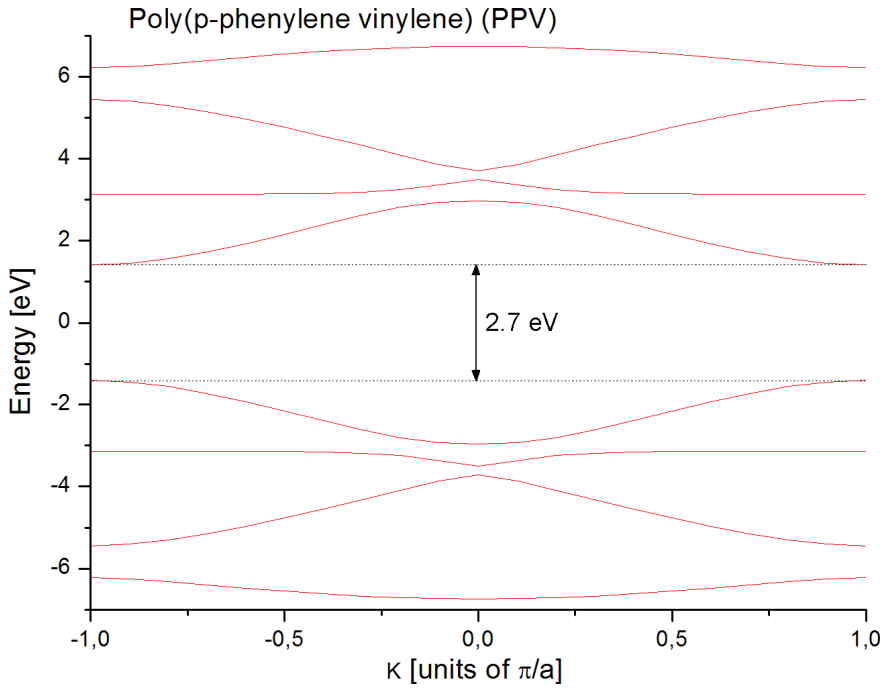

Figure 4.5: The band structure of PPV. The bands are calculated using a lattice constant of 1

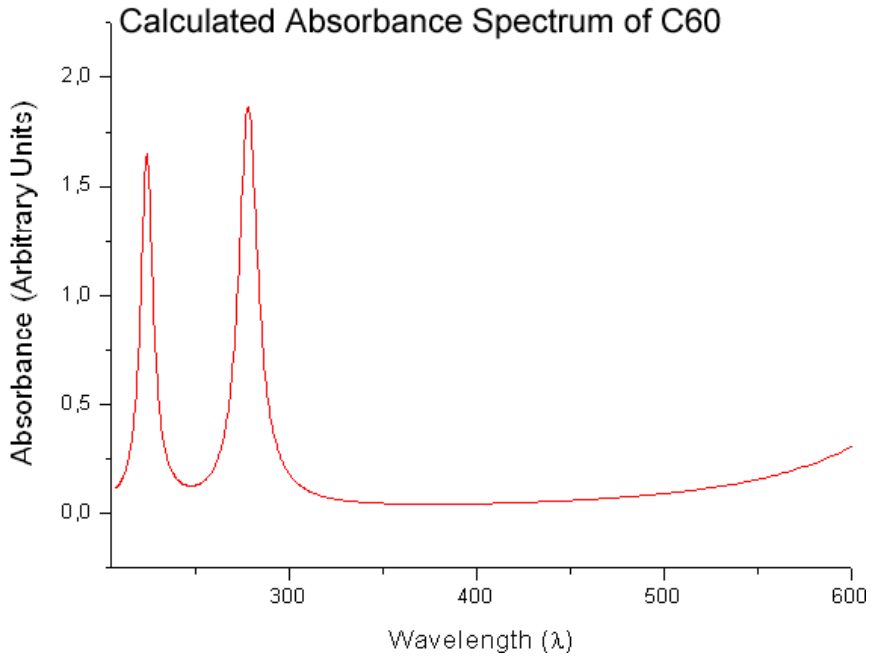

Figure 4.6: The calculated absorbance spectrum of C60

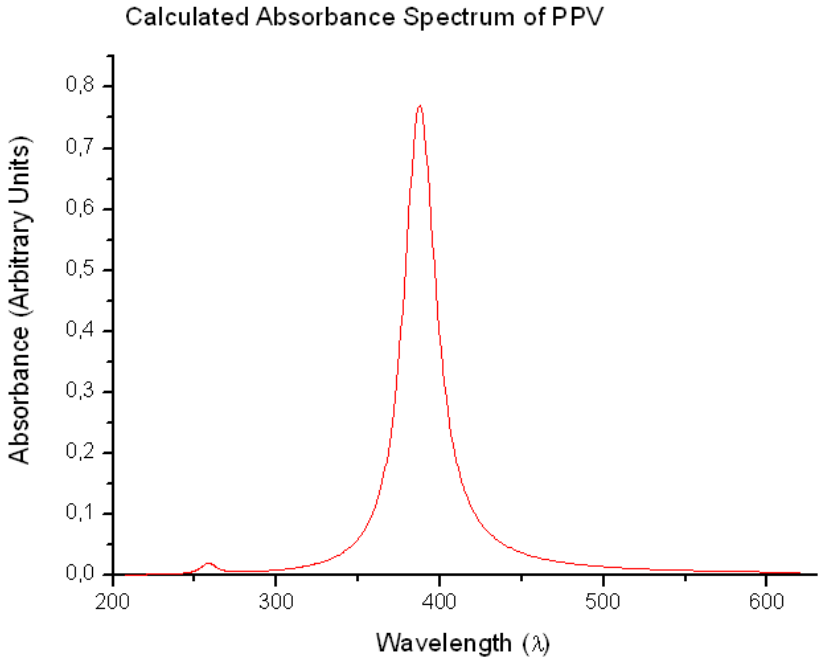

Figure 4.7: The calculated absorbance spectrum of PPV

Chapter 5

Materials Methods

The purpose of this chapter is to clarify the process of the experiments conducted in this project. That includes the various methods used for producing and characterizing the solar cell and its constituents. Finally a list of the compounds used is presented.

5.1 Making the Solar Cell

To make a solar cell, different materials are needed, and the materials have to be processed by different methods. In this section, the processing of the materials will be specified. First of all, a clean glass plate with a thin layer of ITO (Indium Tin Oxide) is needed. These plates are bought from Delta Technologies. The ITO acts as the first part of the solar cell, the first electrode. A bit of the ITO has to be removed, to avoid short-circuiting. This will happen if the two conducting layers of the solar cell touch each other. The ITO that has to be removed is etched away with boiling aqua regia, which is a solution of concentrated hydrochloric acid and concentrated nitric acid. As seen in Figure 5.1, is the lower part of the ITO removed when it has been immersed into the aqua regia for ten seconds. Afterwards is the plate washed in water to clean the plate for remaining aqua regia.

When a solar cell is made, it is important that the materials are clean. To clean the plate, it is first washed with soap; secondly it is put in ultrasonics bath with the solvent acetone, then water and finally ethanol. After the plate have been cleaned with ultra sound, the plate is washed with ethanol and dried with a nitrogen pistol.

5.1.1 Solutions

Two solutions has to be made, a MEH-PPV:PCBM-solution, and a PEDOT:PSS-solution. The concentrations of the different chemicals are described in

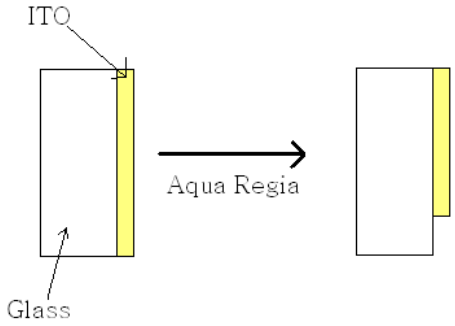

Figure 5.1: A piece of the ITO is etched by the Aqua Regia.

Short name	CAS#
MEH-PPV	138184-36-8
C_{60} PCBM	160848-22-6
THF	109-99-9
PEDOT:PSS	155090-83-8
TWEEN-20	9005-64-5

Table 5.1: The chemicals used for production of the solar cell.

the table Table 5.2 and Table 5.3. MEH-PPV and PCBM is dissolved in THF(Tetrahydrofuran), which is a polar solvent, it is important to be aware, that THF has to be kept in a glass bottle. The MEH-PPV:PCBM-solution has to be treated carefully, the chemical MEH-PPV(PolyPhenylene Venylene) is very light sensitive so it has to be wrapped in silver paper to keep the MEH-PPV from reacting with sunlight. PCBM is added in order to make the dissociation of excitons more efficient.

In the PEDOT:PSS solution, Table 5.3, PEDOT:PSS(0,7%) is used, which means that 0,7% of the solution is PEDOT:PSS, the remaining 99,3% is water. Tween is added to make the solution more viscous.

MEH-PPV	PCBM	THF
50mg	200mg	15ml

Table 5.2: The MEH-PPV-solution made for the solar cell.

PEDOT:PSS(0.7%)	TWEEN-20
1000μl	100μl

Table 5.3: The PEDOT:PSS-solution made for the solar cell.

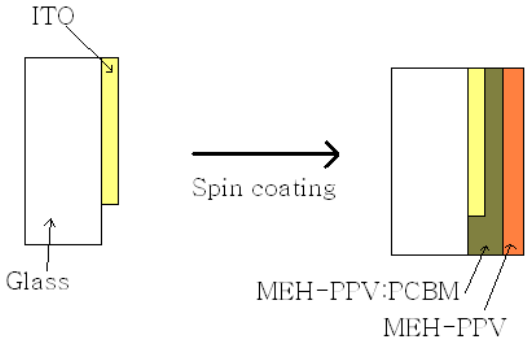

Figure 5.2: A layer of PEDOT:PSS and MEH-PPV is spun on the plate.

5.1.2 Spin Coating

The two solutions have to be spun over the plate. The first layer is PEDOT:PSS. When the PEDOT:PSS has been spun onto the plate it has to be heated in order to evaporate the water from the solution. The second layer is MEH-PPV which functions as the active layer in the solar cell. The PEDOT:PSS layer is spun with 1000 rpm and the MEH-PVP layer is spun with 750 rpm both for 25 seconds. Figure 5.2 shows a model of the structure.

5.1.3 Creating the Calcium and Aluminium Layer

Firstly a calcium layer is needed on the plate, this layer is made to increase the built-in electric field. Secondly the aluminium layer is made, this has the function as the second electrode, also it protects calcium that is a very reactive metal. To create these layers the metals (calcium and aluminium) is evaporated onto the plate and this is done in a vacuum to allow evaporation and make sure that it is a clean evaporation. First a piece of metal is placed in a evaporation boat, the plate is placed above the metal, then the vacuum has to be created. To create such vacuum two pumps are needed. First a primary pump, this is a rotation pump, that will make a pressure of approximately 1×10^{-1} mBar. Secondly the other pump is turned on, this is a diffusion pump and it will make the pressure fall down to 1.5×10^{-4} mBar, which is the least needed to make sure the evaporation will be pure.

First the calcium is evaporated onto the solar cell, an effect of 300 W is set over the evaporation boat containing the calcium, and a layer of calcium

will be created on the cell. To control the size of the layer, a sensor is measuring the amount of calcium evaporated onto the plate. This is done by a plate consisting of crystals, which is set to a resonant frequency. When the evaporated calcium hardens on the crystal plate, the frequency will change. A program can calculate the thickness of the layer by the change in frequency. When the thickness of the calcium layer is approximately 75 nm, the effect is set to 0 W, so the evaporation of the calcium will stop.

Secondly it is needed to vaporize the aluminium. An effect of 250 W is set over the evaporation boat containing the aluminium, this will heat up the aluminium, which will vaporize and thereby create a thin layer of aluminium on the plate above the calcium. When a thickness of approximately 100 nm aluminium has been vaporized on the plate, the pressure is equalized. The solar cell is then taken out of the vacuum chamber and is tested by measuring IV-curves of the solar cell.

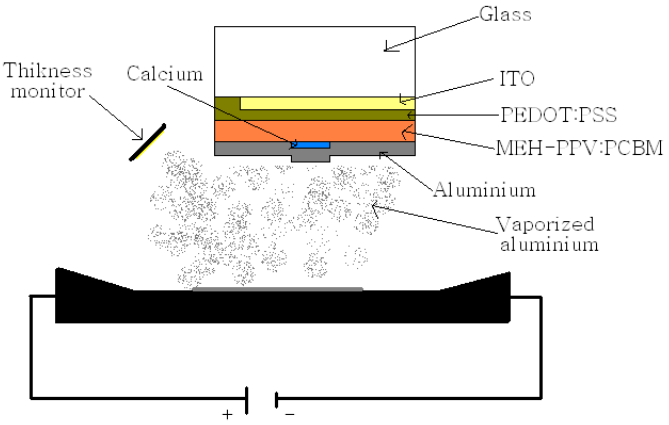

Figure 5.3: Shows what happens inside the vacuum chamber, how the aluminium is vaporized on the solar cell.

The procedure of making a polymer solar cell has now been explained, in this project, different types of polymer solar cells has been made, to find the advantage of the different layers, The different types of solar cells made, is seen in Table 5.4.

5.2 Measuring Absorbance

When absorbance is measured, it is done by a photodetector, able to measure different wavelengths of light, Figure 5.4. The spectrometer used is Ocean Optics Inc. ISS-UV-VIS.

Type		ITO	PEDOT:PSS	MEH-PPV	$PCBM$	Calcium	Aluminium
1		X	X	X	X	X	X
2		X	X	X	X		X
3		X		X	X	X	X
4		X		X	X		X

Table 5.4: Shows the different types of solar cells which will be made.

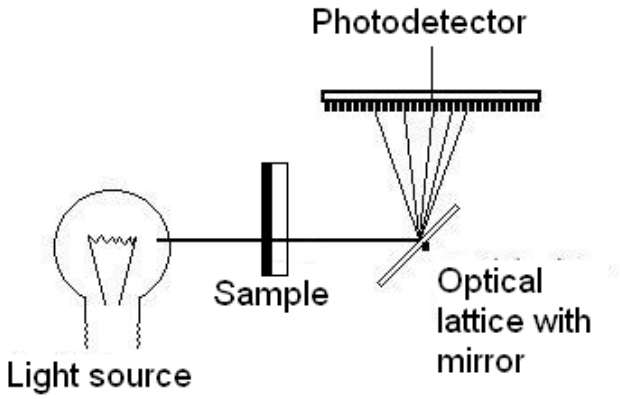

Figure 5.4: A polychromatic light spectrophotometer

A light beam is sent through the sample, and the sample will absorb some of the light. Some of the light will pass through and hit the optical lattice, which will divide the light into different wavelengths and thereby make it possible for the photodetectors to measure which wavelengths has been absorbed and which has not.

When a solar cell is made, absorbance is measured of the MEH-PPV:PCBM and PEDOT:PSS, this is done during the production of the solar cell. When absorbance of the MEH-PPV:PCBM layer is measured, it is with glass, ITO and PEDOT:PSS as reference (If PEDOT:PSS is not used in the solar cell, is it not used as reference). When absorbance of PEDOT:PSS is measured, it is with glass and ITO as reference.

The measurements are made, to find the absorbance of the individual layers, and to see if they absorb too much light, to function as a solar cell.

5.3 Measuring the IV Characteristic

In order to compare various solar cells it is necessary to measure the characteristic values: V_{oc}, I_{sc}, the fill factor and the efficiency, η. All these factors

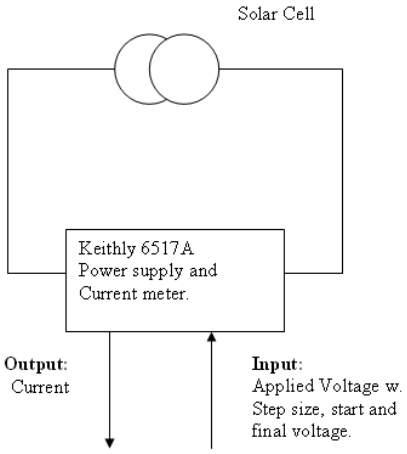

Figure 5.5: The setup for measuring the IV characteristics of solar cells.

can be determined from the IV characteristic of a solar cell and the power-output from the lamp. Therefore an IV characteristic will be performed under illumination and in dark for each solar cell in this project.

The IV characteristic is a measurement of the current as a function of the applied voltage. There are various ways to achieve this. The most simple is with an oscilloscope, as it is able to apply a varying voltage and picture the corresponding current on a screen. It is however not very precise as it was not possible to get data output to a computer.

Therefore a setup with a Keithly model 6517A Electrometer was used. This electrometer is able to supply a voltage and measure the current. Furthermore it is possible to connect it to a computer, which provides the possibility of automatization of the measurements [Group442, 2006]. The setup is displayed in Figure 5.5.

Chapter 6

Results

This chapter presents the results obtained form the experiments, which have been carried out in the laboratory during this project. The chapter is divided into two sections. One presenting the results obtained form the absorbance experiments and another presenting the results from the IV characterization of the solar cells.

6.1 Absorbance

The absorbance of the separate parts of the polymer solar cells has been measured, and are plotted in Figure 6.1.

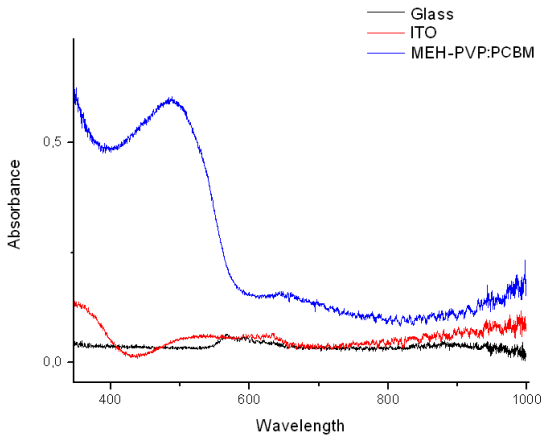

Figure 6.1: The graph shows the absorbance measured of the materials used for the solar cells without PEDOT. When the absorbance of glass is measured, it is with air as reference. For ITO glass is reference. For MEH-PPV:PCBM glass and ITO is reference.

Figure 6.1 shows as expected, that MEH-PPV:PCBM absorbs light at the wavelengths 400nm to some above 550nm with a peak at 500 nm. It also absorbs light with a wavelength below 400nm. ITO and glass does not absorb any light in the visible area and, more importantly, not in the area where MEH-PPV:PCBM absorbs light, this is also expected from Figure 2.7.

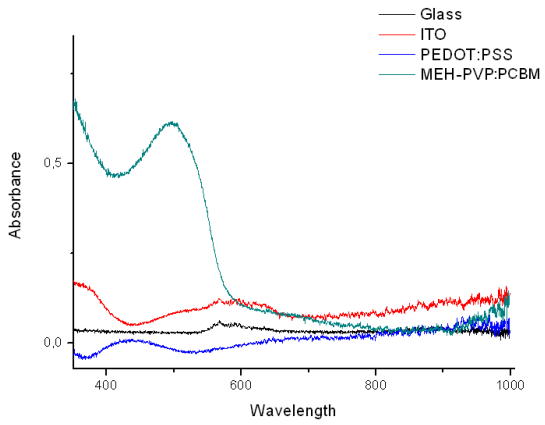

Figure 6.2: The graph shows the absorbance measured of the materials used for the solar cells with PEDOT. When the absorbance of glass is measured, it is with air as reference. For ITO glass is reference. For PEDOT:PSS glas and ITO is reference. For MEH-PPV glas, ITO and PEDOT:PSS is reference.

Figure 6.2 also shows, as in Figure 6.1, that MEH-PPV:PCBM, glass and ITO absorb as expected. Though, when applying PEDOT:PSS to the plate, a negative, and a generally very low, absorbance is shown. The negative absorbance is caused by PEDOT:PSS when glass is used as reference. PEDOT:PSS will remove some of the reflective ability of glass, and thereby make more light pass through. The low absorbance is due to the very thin layer which has been spun over the plate, making PEDOT:PSS absorb only a small amount of light. In the absorbance measurements made in this project, it is seen, that even though PEDOT:PSS has a broad absorbance area, it absorbs almost no light when applied to a glass plate in thin films. This is important, so that none of the light MEH-PPV:PCBM absorbs, will be absorbed by PEDOT:PSS.

6.2 IV characterization

This section presents the IV-curves from the solar cells, which have been analyzed in the laboratory.

Figure 6.3 shows an IV-curve obtained from an ordinary silicon solar cell under illumination. I_{SC}, I_m, V_m, and V_{OC} are marked on the curve.

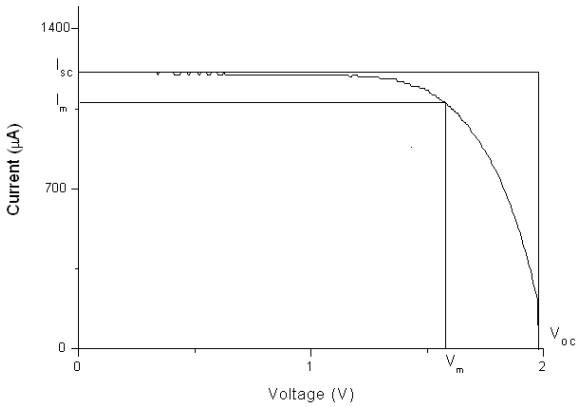

Figure 6.3: A light IV-curve from a silicon solar cell, measured at applied voltage between 0 and 2 V. I_{SC}, I_m, V_m, and V_{OC} is marked on the curve at 12100 μA, 10600 μA, 1.579 *V, and* 1.99 *V, respectively.*

Figure 6.4 and Figure 6.5 show IV-curves from the polymer solar cells that have been made in the laboratory. Both figures display IV-curves from the same five polymer solar cells (A-E) under illumination. Figure 6.4 shows the measured IV-curve from -1 to 1 V and Figure 6.5 from 0 to 1 V. Figure 6.5 is made in order to make it easier to see the details in this interval. Solar cell A-C are made by this group and D-E are made by group 4.42 from Aalborg University.

Solar cell A, D and E are all ITO/MEH-PPV:PCBM/Al solar cells, but they are made from different solutions. Solar cell A is made from the solution described in Section 5.1. The two other solar cells are made from two different solutions where MEH-PPV and PCBM have been dissolved in toluene, D 6.67 g/L and E 16.67 g/L. The ratio between MEH-PPV and PCBM is 20 : 80 for all the polymer solar cells.

Solar cell B and C are both ITO/PEDOT:PSS/MEH-PPV:PCBM/Al solar cells and they are made from the same MEH-PPV:PCBM and PEDOT:PSS solutions.

In Section 5.1 it was stated that solar cells with a calcium layer in between the active and aluminium layer would be produced but unfortunately those polymer solar cells were not functional.

The IV-curves, which were measured in the dark are shown in Figure 6.6 and Figure 6.7. Figure 6.6 shows the IV-curves from solar cell A,C,D, and E. Unfortunately the measurement on solar cell B failed. As it can be seen in Figure 6.6 is it difficult to see any details on the IV-curves from solar cell A,C, and E since the IV-curve from solar cell D dominates the picture. Therefore the IV-curves from solar cell A, C, and E are also displayed in Figure 6.7.

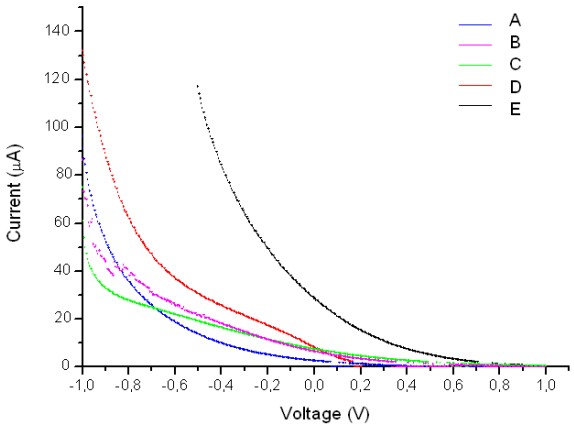

Figure 6.4: Light IV-curves from polymer solar cells A-E, measured at applied voltage between -1 and 1 V. Solar cell A,D, and E are all ITO/MEH-PPV:PCBM/Al solar cells. Solar cell B and C are ITO/PEDOT:PSS/MEH-PPV:PCBM/Al solar cells.

In Figure 6.8 the IV-curve of solar cell B is presented again, but this time I_{SC}, I_m, V_{OC}, and V_m are marked.

In Table 6.1 I_{SC}, I_m, V_{OC}, V_m, P_m, and the fill factor (FF) are listed for all the solar cells.

Type	I_{SC} (μA/cm^2)	V_{OC} (V)	I_m (μA/cm^2)	V_m (V)	P_m (μ W/cm^2)	FF
Si	605	1.99	530	1.579	846.41	0.7
A	2.61	0.47	1.25	0.2	0.25	0.2
B	6.41	0.87	2.39	0.3	0.717	0.129
C	7.44	1.05	3.04	0.35	1.06	0.136
D	8.23	0.415	3.44	0.12	0.413	0.121
E	28.7	1.1	11.8	0.28	3.304	0.104

Table 6.1: The measured I_{SC} and V_{OC} from the silicon solar cell (Si) and the polymer solar cells A-E are listed. Furthermore is the calculated I_m, V_m, P_m and the the fill factor (FF) listed for each solar cell. The unit $\mu A/cm^2$ referrer to the current produced per active area of a solar cell.

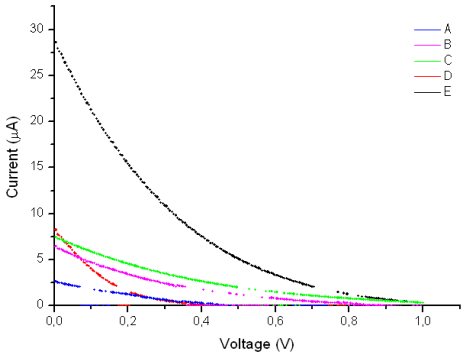

Figure 6.5: Light IV-curves from polymer solar cell A-E, measured at applied voltage between 0 and 1 V. Solar cell A,D, and E are all ITO/MEH-PPV:PCBM/Al solar cells. Solar cell B and C are ITO/PEDOT:PSS/MEH-PPV:PCBM/Al solar cells.

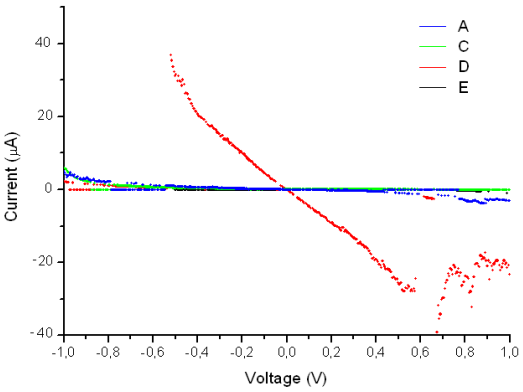

Figure 6.6: Dark IV-curves from polymer solar cell A,C,D, and E measured at applied voltage between -1 and 1. Solar cell. Solar cell A,D, and E are ITO/MEH-PPV:PCBM/Al solar cells and solar cell C is an ITO/PEDOT:PSS/MEH-PPV:PCBM/Al solar cell.

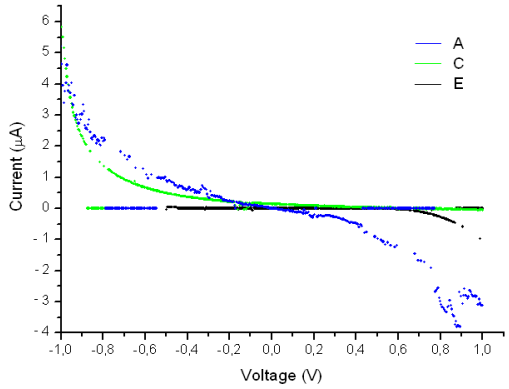

Figure 6.7: Dark IV-curves from polymer solar cell A,C, and E, measured at applied voltage between -1 and 1. Solar cell. Solar cell A and E are ITO/MEH-PPV:PCBM/Al solar cells and solar cell C is an ITO/PEDOT:PSS/MEH-PPV:PCBM/Al solar cell.

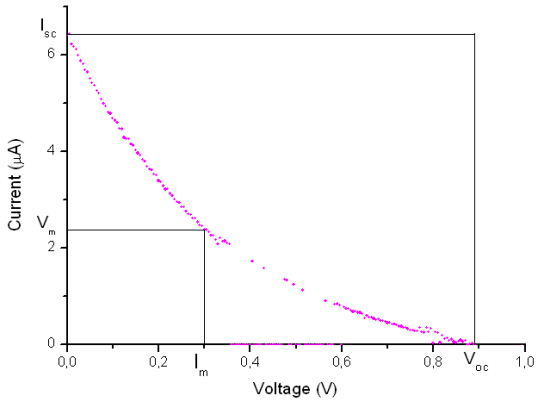

Figure 6.8: Light IV-curve from solar cell B, measured at applied voltages between 0 and 1 voltage. I_{SC}, I_m, V_{OC}, and V_m marked on the curve at 6.41 μA, 2.39 μA, 0.87 V, and 0.3 V, respectively. Solar cell B is an ITO/PEDOT:PSS/MEH-PPV:PCBM/AL solar cell.

Chapter 7

Discussion

This chapter discusses the results obtained from the experiments and the theoretical results obtained from the calculations made by the program. The chapter starts with a discussion of some of the difficulties which was faced in the production of the solar cells. Thereafter a discussion of the IV-curves is made, and finally a discussion of the theoretical results is made.

7.1 Difficulties

During the production of the polymer solar cell, different problems have been faced. Firstly THF that has been used as solvent for PCBM and MEH-PPV had certain difficulties with dissolving the two materials. This made it difficult to spincoat a pure and homogeneous film and this again affects the charge transport of the solar cell. The importance of a high vacuum of 1.5×10^{-4} mBar has also created problems during the process, as the pressure increased during the evaporation of aluminium and calcium. This resulted in an unclean evaporation and a non functional solar cell.

The lifetime of a polymer solar cell was limited, which means that measurements has to be made fast, or the solar cell will die out before any measurements are made. During measurements of IV-curves under illumination, the lamp drastically increases the temperature of the cell. Therefore the cell was not in thermal equilibrium.

All these factors played a great role in the production and measurements of the solar cells. Only a limited number of functional solar cells was produced due to the pressure increasing rapidly under evaporation. The limited lifetime of the cells made it troublesome to conduct reliable measurements of the cells.

7.2 IV Characterization

This part of the discussion will deal with the performance of the analyzed solar cells. As mentioned in Section 6.2 only five functional polymer solar cells were produced. Therefore it is hard to make any conclusions on how the different concepts affect the performance of the polymer solar cell. Even though, the performance of the different solar cells will be compared with each other and analyzed in relation to their structure. All the measured and calculated data form the solar cells can be found in Table 6.1

As it can be seen in Table 6.1 the performance of the silicon solar cell is superior to the polymer solar cell as expected. This superiority is even more clear when comparing the IV-curves, see Figure 6.3 and Figure 6.5. The IV-curve from the silicon solar cell is a curve similar to the curve from the optimal model, described in Section 3.2. This indicated that the silicon solar cell is effective in the dissociation of excitons and in the transport of the charge carrier afterwards. The IV-curves from the polymer solar cells however do not fit to the optimal IV-curve and the reason for this can be hard to explain. One problem could be the charge transport in the active layer, where a bad charge transport will result in a large series resistances. The reason why it is believed that the polymer solar cells ability to transport charges is low is supported by the fact that the solar cells were able to function as a light diode. The introduction of PCBM should increase the electron conductivity of the active layer and thereby lower its ability to emit light when a voltage is applied. This curvature of the IV-curve is also responsible for the low fill factor and P_m of the polymer solar cells, see Figure 6.8.

When comparing solar cell A with solar cell B and C (Figure 6.4 and Figure 6.5) it can be seen that V_{OC} is highest for solar cell B and C. V_{OC} for A, B, and C is 0.47, 0.87, and 1.05 V respectively. The increased voltages are probably caused by the introduction of the PEDOT:PSS layer, due to the difference in work function between ITO and PEDOT:PSS. The observed value of I_{SC} for the three solar cells was 2.61, 6.41, and 7.44 $\mu A/cm^2$ for A, B, and C. As it can be seen the current is more than doubled for solar cell B and C compared to A. This increase is probably a consequence of a better junction at the high work function electrode caused by the PEDOT:PSS layer and the increased open circuit voltages.

When comparing the IV-curves from solar cell B and C, present in Figure 6.4 and Figure 6.5, there is a similar behavior between them. This similar behavior was expected since the two solar cells have been made using the same procedure.

The active layer in solar cell D and E have been made from a solution where MEH-PPV and PCBM was dissolved in toluene and that might have had an impact on the active layer. When comparing D and E with A is it clear that I_{SC} was increased significantly. I_{SC} was increased from 2.61

$\mu A/cm^2$ for solar cell A to 8.23 and 28.7 $\mu A/cm^2$ for solar cell D and E. This increase may indicate that MEH-PPV and PCBM are dissolved more homogeneously in toluene than in THF. The concentration difference in the two solutions used in solar cell D and E is probably the reason why I_{SC} is highest in solar cell E. Since the high concentration of MEH-PPV:PCBM will give a better absorbing layer and thereby increasing the amount of produced charges. Both layers were spin coated at 750 rpm.

V_{OC} is almost the same for solar cell A and D, 0.47 and 0.415 V, as expected since no improvements have been made at any of the electrodes. V_{OC} of solar cell E is the highest measured for all the polymer solar cells, 1.1 V. This high V_{OC} is unexpected since no improvements have been made in order to increase the built-in potential difference. The origin for this high V_{OC} could be an exceptional high work function of the ITO layer.

The dark IV-curves from the polymer solar cells are presented in Figure 6.6 and Figure 6.7. As it can be seen the dark IV-curve for solar cell D differs from the rest. The reason for this can be that the dark IV-curves was not measured in absolute darkness and that might have affected the measurement. The rest of the dark IV-curves show low values of voltages and currents as expected.

7.3 Calculations

The band gap of PPV was calculated to 2.7 eV. This is not in too well accordance with the spectrum of the lamp which peaks at 500 nm. 2.7 eV is a large bandgap for a solar cell, because only light with wavelengths shorter than 460 nm are absorbed and the spectrum of the sun is most intense at wavelengths between 400 nm and 550 nm. The bandgap of PPV has been measured to 2.14 eV by [Chambers and Selmic, 2005]. The too large calculated band gap can be ascribed to the rather rough approximations made in the Simple Hückel Method. In a more refined model the resonance integral between atoms that are not directly bonded should not simply be zero. Also, the resonance integral of all directly bonded atoms is assumed to be equal. This does not appreciate the small variations in the local spatial environment of the atoms.

The calculated absorbance spectrum of PCBM is blue shifted by about 30 nm compared to the measured spectrum. Again this can be ascribed to the rough approximations made. The calculated absorbance spectrum of PPV has a peak at 390 nm. This is about 100 nm blue shifted compared to the measured absorbance spectrum of PPV which peaks at about 480 nm. This could be due to the calculated band gap being too large.

Chapter 8

Conclusion

In this project calculations of band structures and absorbance spectra of conjugated polymers and fullerenes have been made and different types of polymer solar cells have been produced. This chapter will be used to conclude on the problem statement in Section 2.8.

The program EBCalc have been developed in this project and its ability to calculate band structures and absorbance spectra have been used to calculate band structures and absorbance spectra for the conjugated polymers PPP and PPV. Furthermore an absorbance spectrum of the fullerene C_{60} has been calculated. The calculated band structures and absorbance spectra were compared with experimentally obtained data. This comparison shows a reasonable accuracy of the calculated data in spite of the rough approximations that have been made in the model used for the calculation.

Only a limited number of functional polymer solar cells was produced and analyzed. The purpose with this polymer solar cell production was to find a relation between changes at the electrodes and the performance of the solar cells. Only the introduction of a PEDOT:PSS layer in between the ITO and the active layer succeed. This introduction of a PEDOT:PSS layer was reflected in the performance of the solar cells by an increase in the I_{SC} and V_{OC}. Even though this increase was observed more experiments have to be made before it can be concluded, that an introduction of PEDOT:PSS layer in a ITO/MEH-PPV:PCBM/Al solar cell will increase I_{SC} and V_{OC}. Beside this, results obtained by this group and group 4.42 from Aalborg University indicates the dissolving of MEH-PPV and PCBM in toluene gives at better active layer than if they were dissolved in THF. This statement is also based on a limited amount of data and therefore more experiments must be carried out before this can be verified.

Appendix A

Doping

Doping in semiconductor production refer to the process of intentionally introducing impurities into pure semiconductor in order to alter the conductivity of the semiconductor. Depending of the impurity the doping process is divided into two classes: n- or p-doping.

A.1 N-doping

The n-doping of semiconductors refer to a doping process of the semiconductor which increases the density of the electrons relative to that of the holes. The letter n in n-doping is used since the majority of charge carriers are negative.

A perfect silicon crystal will be used as the starting point for the explanation of n-doping. Silicon is a Group IV atom; hence it has four outer-shell or valence electrons. In silicon crystals these four valence electrons are used to form four covalent bonds with four neighbouring atoms.

When an impurity in the form of a Group V atom is introduced into the crystal it will use four of its five valence electrons to form covalent bonds with four neighboring silicon atoms, Figure A.1. The fifth valence electron will not be used in a covalent bond and it will therefore be nearly free, only held loosely in a Coulombic bond state with the parent atom. The energy of this nearly free electron lies in between the valence and conducting bands of the semiconductor, see Figure A.1. Such an impurity atom is called a donor atom because it donates an electron to the lattice.[Nelson, 2003]

It is relatively easy to ionize a donor atom because the gab between the conduction band and donor bound level is small, typically in the order of 0.05 eV. The average energy of an electron at room temperature is about $k_B \cdot T = 0.025$ eV. Therefore only a small amount of thermic energy is needed to excite the electron from the donor bound level to the conduction band and thereby increasing the conductivity of the semiconductor.[Kittel, 2005]

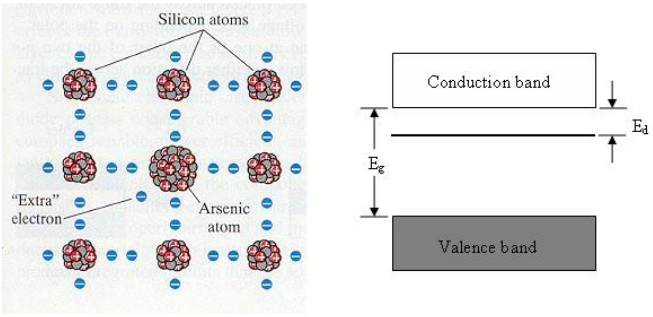

Figure A.1: (Left)Two-dimensional silicon crystal which has been n-doped with Arsenic. (Right) Band structure of an n-doped semiconductor. Modified from [O'Connell, 2006]

A.2 P-doping

P-doped semiconductors are semiconductors where the density of holes in relation to electrons has been increased. The letter p is used to mark this type of doping since the charge carriers are positive electron holes.

A perfect silicon crystal will also be used as the starting point for the explanation of this type of doping. The difference between n- and p-type doping lies in the type of atoms used to dope the crystals. To p-dope a silicon crystal a Group III atom is used, instead of a Group V atom as in n-doping. A Group III atom contains one valence electron less than silicon, which makes it unable to form covalent bonds to all of its four nearest neighbor atoms, Figure A.2. Therefore only three of the neighboring silicon atoms will form covalent bonds with the impurity atom. The fourth bond can be formed if the impurity atom is ionized by accepting an electron from a silicon atom elsewhere in the lattice, hence the atom is called an acceptor atom. Such an ionization of the impurity atom releases an electron hole into the valence band. The energy of the ionized state is a small amount higher than the energy of the valence band electron, resulting in an introduction of an energy level in between the valence and conducting band, see Figure A.2. The size of this new energy gab is about 0.05 eV which make a thermic excitation a room temperature possible.[Nelson, 2003]

These electron holes are capable of carrying a current if an electric field is applied to the semiconductor. Therefore the presence of these electron holes increases the conductivity of the semiconductor.[Serway and Jewett, 2004]

The amount of impurities which is needed to increase the conductivity of a semiconductor is very small. In the p-doping of silicon, one boron atom to 10^5 silicon atoms increases the conductivity of pure silicon at room temperature by at factor of 10^3.[Kittel, 2005]

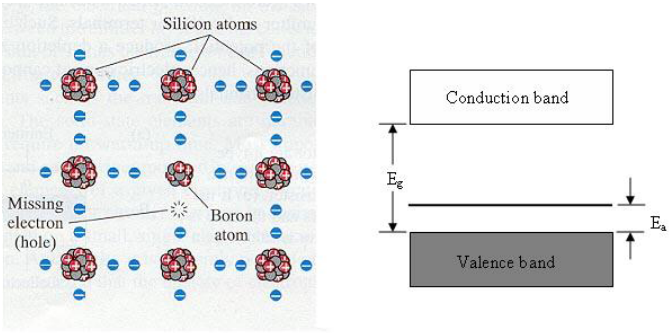

Figure A.2: (Left)Two-dimensional silicon crystal which has been p-doped with boron. (Right) Band structure of a p-doped semiconductor. Modified from [O'Connell, 2006]

Appendix B

Junctions

The pn junction in a silicon solar cell was shortly described in Section 1.2. This appendix will give a more extended description of the PN junction. The following terms will be treated: Built-in potential barrier, built-in electric field, and space charge width.

B.1 Built-in potential barrier

Lets consider a single crystal semiconductor where one region of the crystal is p-doped and another is n-doped. For simplicity the doping concentration in each region are uniform and there is an abrupt change in the doping at the junction. This type of junction is normally referred to as a step junction.[Neamen, 1992]

At the interface between the two regions there exists a high density gradient in both electron and hole concentration. This means that electrons will start to diffuse from the n-doped region into the p-doped region and vice versa. When electrons from the n-doped region start to diffuse into the p-doped region they leave positively charged donor atoms behind in the n-doped region. The hole from the p-doped region leave negatively charged acceptor atoms behind in the p-doped region. The diffusion continues until a thermal equilibrium is established and a net positively and negatively charged region is created. These two regions are referred to as the space charged region or the depletion region since all the free charge carriers are swept out of this region. When this thermal equilibrium is reached the Fermi levels have aligned, see Figure B.1[Neamen, 1992]

As it can be seen in Figure B.1 are the conduction and valence band energies bend through the space charge region. This bending occurs since the relative position of the conduction and valence bands with respect to the Fermi levels changes between the p- and n-regions.

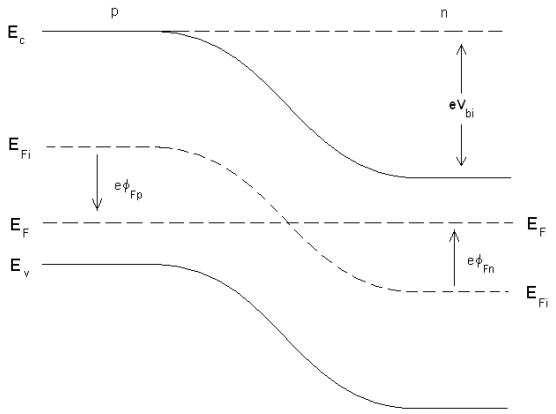

Figure B.1: The energy-band diagram for a pn junction in thermic equilibrium.

Electrons in the conduction band in the n-region see a potential barrier if they try to move into the conduction band in the p-region. This potential barrier is referred to as the built-in potential barrier and is denoted V_{bi}. Holes in the p-region meet the same barrier when they try to move into the valence band in the n-region.[Neamen, 1992]

To determine the built-in potential barrier it is necessary to look at the intrinsic Fermi level, which is equidistant from the conduction band edge through the junction. The built-in potential barrier is equal to the difference between the intrinsic Fermi levels in the p- and n-region.[Neamen, 1992] The two potentials ϕ_{Fp} and ϕ_{Fn} is defined as shown in Figure B.1, which means V_{bi} is equal to:

$$V_{bi} =\mid \phi_{Fn} \mid + \mid \phi_{Fp} \mid \tag{B.1}$$

In order to determine ϕ_{Fp} it is necessary to look at the electron concentration (n_0) in the conduction band in the n-region, which is given by:

$$n_0 = N_c exp[(E_F - E_c)/kT] \tag{B.2}$$

N_c is the effective density of state function in the conducting band. E_F is the energy at the Fermi level and E_c is the energy at the conduction band. T is the temperature of the semiconductor and k is Boltzmanns constant.

The electron concentration in the conducting band of an intrinsic semiconductor is give by:

$$n_i = N_c exp[\frac{(E_c - E_{Fi})}{kT}] \tag{B.3}$$

By using Equation B.3 Equation B.2 can be written in the form:

$$n_0 = n_i exp[\frac{(E_F - E_{Fi})}{kT}] \tag{B.4}$$

Where E_{Fi} is the intrinsic Fermi energy. The potential ϕ_{Fn} can then be defined as:

$$e\phi_{Fn} = E_{Fi} - E_F \tag{B.5}$$

e is the elementary charge. When Figure B.5 is used and n_0 set equal to N_d, which is the net donor concentration in the n-region, ϕ_{Fn} is given by:

$$\phi_{Fn} = \frac{-kT}{e} ln\left(\frac{N_d}{n_i}\right) \tag{B.6}$$

An expression for ϕ_{Fp} can be derived in a similar way:

$$\phi_{Fp} = \frac{kT}{e} ln\left(\frac{N_a}{n_i}\right) \tag{B.7}$$

N_a is the net acceptor concentration in the p-region. Finally the built-in potential barrier form the step junction is found by substituting Equation B.6 and Equation B.7 into Equation B.8:

$$V_{bi} = \frac{kT}{e} ln\left(\frac{N_a N_d}{n_i^2}\right) \tag{B.8}$$

B.2 Electric Field

This section will be used to drive an expression for the electric field, which arise due to the creation of positive and negative space charge densities. Figure B.2 illustrates the volume charge density distribution. It is assumed that the doping is uniform and that the space charge regions abruptly ends at x equal to $+x_n$ and $-x_p$.

The electric field can be determined by using Poisson's equation which for a one-dimensional situation is:

$$\frac{d^2\phi(x)}{dx^2} = \frac{-\rho(x)}{\epsilon_s} = -\frac{dE(x)}{dx} \tag{B.9}$$

$\phi(x)$ is the electric potential, E(x) is the electric field, ϵ_s is the permittivity of the semiconductor and $\rho(x)$ is the volume charge density. $\rho(x)$ is only present in the deletion zone, see Figure B.2, and therefore it can be expressed in the following manner:

$$\rho(x) = -eN_a \qquad -x_p < x < 0 \tag{B.10}$$

$$\rho(x) = eN_a \qquad 0 < x < x_n \tag{B.11}$$

An expression for the electric field in the two region can be driven by integrating Equation B.9 and using the boundary conditions for the electric

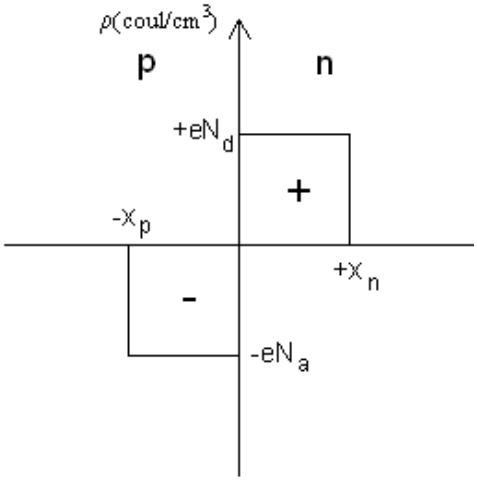

Figure B.2: The energy-band diagram for a pn junction in thermic equilibrium.

field, E=0 for -x_p=x=x_n. The electric field in the p-region can then written as:

$$E = \frac{-eN_a}{\epsilon_s}(x + x_p) \qquad -x_p < x < 0 \tag{B.12}$$

A similar expressing describes the electric field in the n-region:

$$E = \frac{-eN_a}{\epsilon_s}(x_n - x) \qquad 0 < x < x_n \tag{B.13}$$

Since the electric field is continuous at the junction, or at x= 0, a relation between the width of the two space charge regions can be formed by setting Equation B.12 and Equation B.13 equal to each other at $x = 0$

$$N_a x_p = N_d x_n \tag{B.14}$$

This relation will later be used to drive an expression for the space charge width.

B.3 Potential

In this section an expression for the built-in potential barrier will be driven.

The potential in the junction is found by integrating the electric field in the two regions and using the boundary conditions. When determine the boundary conditions for the potential is it important to be aware, that it is only the potential difference through the junction that is the important parameter. Therefore the potential is sat to zero at x=-x_p. Furthermore the

potential is a continuous function through the depletion zone, which mean the integrated electric fields are equal to each other at x=0. The expression for the potential in the two regions i therefore given by:

$$\phi(x) = \frac{eN_a}{2\epsilon_s}(x + x_p)^2 \qquad -x_p < x < 0 \tag{B.15}$$

and

$$\phi(x) = \frac{eN_d}{\epsilon_s}\left(x_n x - \frac{x^2}{2}\right) + \frac{eN_a}{2\epsilon_s}x_p^2 \qquad 0 < x < x_n \tag{B.16}$$

From Equation B.16 is it possible to calculate the size of the potential barrier since it is equal to the potential at $x = x_n$.

$$V_{bi} =\mid \phi(x = x_n) \mid = \frac{e}{2\epsilon_s}(N_d x^n + N_a x_p^2) \tag{B.17}$$

B.4 Space Charge Width

This section will utilize some of the expression that have been driven in the two previous section to calculate the space charge width of a made-up pn junction.

Firstly an expression for the space charge width in the n-region will be driven. Equation B.14 can be rewritten to give:

$$x_p = \frac{N_d x_n}{N_a} \tag{B.18}$$

By substituting Equation B.14 into Equation B.17 and solving for x_n following expression for the space charge width in the n-region can be driven:

$$x_n = \left(\frac{2\epsilon_s V_{bi}}{e}\left[\frac{N_a}{N_d}\right]\left[\frac{1}{N_a + N_d}\right]\right)^{\frac{1}{2}} \tag{B.19}$$

An expression for the space charge width in the p-region can be driven a similarly way to yield:

$$x_p = \left(\frac{2\epsilon_s V_{bi}}{e}\left[\frac{N_d}{N_a}\right]\left[\frac{1}{N_a + N_d}\right]\right)^{\frac{1}{2}} \tag{B.20}$$

The total space charge width W is the sum of Equation B.19 and Equation B.20:

$$W = \left(\frac{2\epsilon_s V_{bi}}{e}\left[\frac{N_a + N_d}{N_a N_d}\right]\right)^{\frac{1}{2}} \tag{B.21}$$

V_{bi} can be determined by Equation B.8.

Lets consider a silicon pn junction at T= $300K$ with the doping densities $N_a = 10^{16} cm^{-3}$ and $N_d = 10^{15} cm^{-3}$, and then calculate the space charge width.

Firstly the size of the built-in potential barrier (V_{bi}) have to be determined by using Equation B.8. At this temperature is the commonly used value of n_i $1.5 \cdot 10^{10} cm^{-3}$. The size of the built-in potential barrier is then given by:

$$V_{bi} = 0.0259 ln \left[\frac{(10^{16})(10^{15})}{(1.5 \cdot 10^{10})^2} \right] = 0.635V \tag{B.22}$$

The space charge width of the pn junction is calculated by using Equation B.21. The permittivity (ϵ_s) for silicon is $1.035 \cdot 10^{-12}$ F/m.

$$W = \left(\frac{2 \cdot 1.035 \cdot 10^{-12} \cdot 0.635}{1.6 \cdot 10^{-19}} \left[\frac{10^{16} + 10^{15}}{10^{16} \cdot 10^{15}} \right] \right)^{\frac{1}{2}} = 951nm \tag{B.23}$$

Using Equation B.19 and Equation B.20, the width in the two regions can found. x_p=$0.864 \mu m$ and $x_p = 0.086$ μm.

Bibliography

[Alvarado et al., 1998] Alvarado, S. F., Seidler, P. F., Lidzey, D. G., and Bradley, D. D. C. (1998). Direct determination of the exciton binding energy of conjugated polymers using a scanning tunneling microscope. *Physical Review Letters*.

[American Dye Source, 2006] American Dye Source, I. (2006). Light emitting homopolymer for oled and pled devices. `http://www.adsdyes.com/products/pdf/homopolymers/ADS200RE_DATA.pdf`.

[Archer and Hill, 2001] Archer, M. D. and Hill, R. (2001). *Clean Electricity From Photovoltaics*. Imperial College Press.

[Boman, 1995] Boman, M. (1995). *Electronic Structure Calculations of Conjugated Polymers, Metal/Polymer Interfaces, and Fulleride Polymers*. Linköping.

[Britannica, 2006] Britannica, E. (2006). Solar energy. `http://search.eb.com/eb/article-9068559`.

[Britannica.com, 2006] Britannica.com (2006). Conjugated polymers. `http://search.eb.com/eb/article-231396`.

[Carlberg, 1996] Carlberg, C. (1996). *Electrochemistry of Conjugated Polymers*. Linköping.

[Chambers and Selmic, 2005] Chambers, D. K. and Selmic, S. (2005). Advanced characterization of the electronic structure of meh-ppv. *Materials Research Society*.

[CRC, 2006] CRC (2006). Handbook of chemistry and physics. `http://http://www.hbcpnetbase.com/`.

[Elektronikbutikken, 2006] Elektronikbutikken, Vesterbrogade, A. C. (2006). Solpaneler cis. `http://solkraft.dk`.

[for Testing and (ASTM), 1999] for Testing, A. S. and (ASTM), M. (1999). Solar spectral irradiance. `http://rredc.nrel.gov/solar/spectra/am1.5/`.

[Group442, 2006] Group442 (2006). Group 442. of Aalborg University.

[Kittel, 2005] Kittel, C. (2005). *Introduction to Solid State Physics*. Wiley.

[Krebs, 2006] Krebs, F. (2006). Risoe. `www.risoe.dk`.

[Krebs et al., 2004] Krebs, F. C., Alstrup, J., Spanggaard, H., Larsen, K., and Kold, E. (2004). Production of large-area polymer solar cells by industrial silk screen printing, lifetime considerations and lamination with polyethyleneterephthalate. *Solar Energy Materials ans Solar Cells*.

[Krebs et al., 2005] Krebs, F. C., Carlé, J. E., Cruys-Bagger, N., Andersen, M., Lilliedal, M. R., and ans Soren Hvidt, M. A. H. (2005). Lifetime of organic photovoltaics: photochemistry, atmosphere effects and barrier layer in ito-mehppv:pcbm-aluminium devices. *Solar Energy Materials ans Solar Cells*.

[Lewars, 2004] Lewars, E. G. (2004). *Computational Chemistry*. Kluwer Academic Publishers.

[Mihailetchi et al., 2003] Mihailetchi, V. D., Blom, P. W. M., Hummelen, J. C., and Rispens, M. T. (2003). Cathode dependence of the open-circuit voltage of polymer:fullerene bulk heterojunction solar cells. *American Institute of Physics*.

[Neamen, 1992] Neamen, C. A. (1992). *Semiconductor physics and devices*. IRWIN.

[Nelson, 2003] Nelson, J. (2003). *The Physics of Solar Cells*. Imperial College Press.

[Norrman and Krebs, 2006] Norrman, K. and Krebs, F. C. (2006). Lifetime of organic photovoltaics: Using tof-sims and $^{18}o_2$ isotopic labelling to characterise chemical degradation mechanisms. *Solar Energy Materials ans Solar Cells*.

[O'Connell, 2006] O'Connell, R. W. (2006). Doping. `http://www.astro.virginia.edu/class/oconnell/astr511/lec11-f03.html`.

[Park et al., 1996] Park, Y., Choong, V., Gao, Y., Hsieh, B. R., and Tand, C. W. (1996). Work function of indium tin oxide transparent conductor measured by photoelectron spectroscopy. *American Insitute of Physics*.

[Press et al., 2002] Press, W. H., Teukolsky, S. A., Vetterling, W. T., and Flannery, B. P. (2002). *Numerical Recipes in C++*. Cambridge University Press.

[Serway and Jewett, 2004] Serway and Jewett (2004). *Physics for Scientists and Engineers*. Thomson Books/Cole.

[Shah et al., 1999] Shah, A., Tscharner, R., Wyrsch, N., and Keppner, H. (1999). Photovoltaic technology: The case for thin-film solar cells. *Science Vol 285*.

[Sigma-Aldrich, 2006] Sigma-Aldrich, C. (2006). Sigma-aldrich. `http://www.sigmaaldrich.com`.

[Spanggaard and Krebs, 2004] Spanggaard, H. and Krebs, F. C. (2004). A brief history of the development of organic and polymeric photovoltaics. *science direct*.

[Yang et al., 2000] Yang, J., Shalish, I., and Shapire, Y. (2000). Photoinduced charge carriers at surfaces and interfaces of poly [2-methoxy-5-(2'-ethyl-hexyloxy)-1,4-phenylene vinylene] with au and gaas. *Physical Review B*.

[Zumdahl, 2003] Zumdahl, Z. . (2003). *Chemistry*. Houghton Mifflin.